Unmanned Systems, Vol. 14, No. 3 (2026) 669–688

DOI: 10.1142/S2301385026410128

UNMANNED SYSTEMS
https://www.worldscientific.com/worldscinet/us

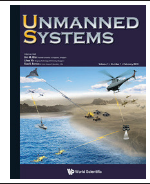

Discrete-Time Extremum-Seeking Control for Nonconvex MISO Hammerstein Systems Using Stochastic Dithers

Xing-Min Chen [*,§], Chao Gao [†,¶], Ying Tan [‡,‖]

[*]School of Mathematical Sciences,
Dalian University of Technology, Dalian,
Liaoning 116024, P. R. China

[†]Department of Basic Courses Teaching, Dalian,
Polytechnic University, Dalian, Liaoning 116034, P. R. China

[‡]School of Electrical, Mechanical and Infrastructure Engineering,
The University of Melbourne, Melbourne VIC 3010, Australia

This paper presents a discrete-time extremum seeking control (ESC) scheme for multi-input single-output (MISO) Hammerstein systems with unknown linear dynamics and a multi-input multi-output (MIMO) cost function. The steady-state cost function may have multiple extrema and, combined with the linear dynamics, exhibits complex behavior; it is assumed to be differentiable, nonconvex, and accessible only via noisy, dynamically filtered sensor measurements. The proposed algorithm integrates stochastic dithers with a stochastic approximation algorithm with expanding truncations (SAAWET), ensuring bounded iterates and closed-loop stability under unmodeled sensor dynamics. Convergence to the set of stationary points of the composite cost function is established from arbitrary initial conditions. The framework extends discrete-time ESC theory to nonconvex, high-dimensional settings with measurement noise and dynamic sensing, providing a rigorous foundation for real-time optimization of nonlinear dynamic systems.

Keywords: Extremum seeking control; MISO Hammerstein systems; randomized gradient-free optimization; stochastic approximation.

1. Introduction

Extremum seeking control (ESC) is a model-free control strategy that searches for the extremum of an unknown objective using real-time input–output measurements and designed perturbations to estimate the gradient in static systems [1]. For dynamic systems, ESC can be extended by exploiting a timescale separation between the fast plant dynamics and the slow adaptation loop to construct an input-to-steady-state-output cost for optimization [2]. As performance optimization is often desired in engineering, ES algorithms have attracted significant attention due to their success across diverse domains, including robotics and maximum power point tracking (MPPT) in wind turbines [3, 4]. This practical success has, in turn, motivated extensive theoretical research aimed at better understanding ES properties and ensuring reliable performance.

In continuous-time ESC, it is usually assumed that the cost function is convex, which guarantees a unique global optimum and convergence from a broad range of initial conditions [5]. In practice, many systems have nonconvex cost functions with multiple local optima. The potential of ESC algorithms in nonconvex static optimization [6] and dynamic optimization [7] has received significant attention in recent years. Classical ESC methods either rely on carefully chosen initial conditions to remain in the basin of attraction of a local optimum [2] or employ computationally expensive global optimization techniques [8].

Received 12 November 2025; Accepted 1 April 2026; Published 13 May 2026. This paper was recommended for publication in its revised form by Special Issues Editors, Jie Chen, Ben M. Chen, and Zongli Lin.
Email Addresses: [§]xmchen@dlut.edu.cn, [¶]gaochao@dlpu.edu.cn, [‖]yingt@unimelb.edu.au
[§]Corresponding author.

In many of the existing ESC, dither signals are used to perturb the system and estimate gradients. Reducing the dither amplitude to zero can compromise robustness, whereas maintaining nonzero dithers ensures stability but limits convergence to a neighborhood of the optimum [8, Remark 9].

Most modern control systems are digitally implemented, motivating the design of discrete-time ESC. Existing results focus primarily on single-input single-output (SISO) systems with convex cost functions and provide only local or semi-global convergence guarantees under stochastic dithers [9–12]. For multi-input single-output (MISO) discrete-time systems with nonconvex cost functions, multiple input configurations can achieve the same optimum, forming a set of local optima. Convergence from arbitrary initial conditions is challenging due to stochastic perturbations and nonlinear interactions, and few results rigorously address this problem.

This paper considers discrete-time MISO Hammerstein systems with unknown linear dynamics and a vector-valued static nonlinearity. The cost function is multi-input multi-output (MIMO), unknown, differentiable, and may have multiple maxima, minima, and saddle points. Only vector-valued noisy measurements are available through digital sensors, which themselves exhibit dynamic behavior. For example, a set of temperature sensors in a room heated by multiple heaters measures temperatures that depend on all heater inputs, while the sensors' thermal time constants introduce filtering and delay. This combination of MISO linear dynamics, MIMO cost, high-dimensional inputs, multiple critical points, and unmodeled sensor dynamics makes conventional gradient-based or exhaustive optimization infeasible. Designing a controller in this context is particularly challenging because the algorithm must operate safely in real time, cope with distorted measurements, and handle multiple local minima, maxima, or saddle points without knowledge of the underlying system parameters.

To address these challenges, the paper proposes an ESC algorithm inspired by stochastic approximation algorithm with expanding truncations (SAAWET). The algorithm injects stochastic perturbations into the inputs to systematically explore the high-dimensional input space while ensuring bounded iterates and maintaining closed-loop stability. This algorithm guarantees convergence to stationary points of the composite multi-input, multi-output cost function. A stationary point is a point where the gradient of the cost function is zero, which may correspond to a local extremum — that is, a local maximum or minimum — or a saddle point. Designing a model-free ESC that converges to a specific extremum is extremely challenging, particularly for complex Hammerstein systems in which the cost function and LTI dynamics are unknown and analytically intractable, as illustrated in Remark 4. Consequently, convergence to stationary points is the most achievable guarantee in such settings.

Despite this limitation, convergence to stationary points remains practically meaningful in many engineering applications — such as HVAC systems, robotic manipulators interacting with human operators, or other multi-input, complex control systems — where the system is too difficult to model, yet all stationary points are safe and stable. In these settings, stationary points often correspond to operationally feasible and predictable regimes. Even when they do not coincide with a desired extremum, identifying these points allows engineers to maintain stable system behavior and make informed adjustments in systems that are otherwise too complex to model.

Moreover, under an additional assumption — for example, knowledge of the sign of the steady-state input–output gain — the ESC algorithm can be guided toward desirable operating points. In this context, stationary solutions can be interpreted within a multi-objective framework, enabling the identification of Pareto-optimal solutions, where no performance criterion can be improved without degrading another. This highlights that, under this additional assumption, the ESC algorithm does not merely identify stationary points but can actively select Pareto-optimal solutions, providing a principled way to achieve balanced performance in complex engineering systems.

The main contributions of this paper are as follows:

(1) We develop a discrete-time ESC algorithm for multi-input Hammerstein systems with nonconvex cost functions. By carefully designing a stochastic perturbation, the algorithm systematically explores the input space and estimates the necessary information for optimization. Under very weak assumptions on the system and cost function, the iterates of the algorithm converge almost surely to stationary points. This provides a rigorous guarantee of stability and convergence even in the presence of nonconvexity and minimal prior knowledge of the system.
(2) We integrate the SAAWET into the ESC framework and extend it to multi-input Hammerstein systems. This integration ensures that the iterates remain bounded and that the algorithm systematically explores the input space, which is essential for reliable estimation in dynamic nonlinear systems. By doing so, SAAWET provides a rigorous foundation for convergence analysis, enabling almost-sure convergence guarantees even in stochastic, nonconvex multi-input settings.
(3) With additional knowledge of the system, the proposed method can converge to a Pareto-optimal solution, demonstrating its potential for multi-objective optimization in complex MISO Hammerstein systems.

This paper is arranged as follows. Section 2 formulates the ESC problem for MISO Hammerstein systems. Section 3 presents the proposed SAAWET-based ESC algorithm. Section 4 establishes the almost sure convergence of the algorithm. Section 5 provides a simulation study to demonstrate its effectiveness. Section 6 concludes the paper.

2. Problem Formulation

2.1. *Multi-objective optimization for MISO Hammerstein systems*

Consider a MISO Hammerstein system, where a multi-objective cost function is connected to a linear time-invariant (LTI) system. At discrete time instants $k = 1, 2, \ldots$, the m-dimensional control input $\boldsymbol{u}_k \in \mathbb{R}^m$ passes through a static nonlinear block $\boldsymbol{J}(\cdot)$ to produce the intermediate signal $\boldsymbol{v}_k$:

$$\boldsymbol{v}_k = \boldsymbol{J}(\boldsymbol{u}_k), \tag{1}$$

where $\boldsymbol{J} : \mathbb{R}^m \to \mathbb{R}^l$ is a continuous vector-valued mapping,

$$\boldsymbol{J}(\boldsymbol{u}) = [J_1(\boldsymbol{u}), \ldots, J_l(\boldsymbol{u})]^\top,$$

with each $J_i(\cdot)$ representing a distinct performance objective. The corresponding multi-objective optimization problem is

$$\min_{\boldsymbol{u}\in U} \boldsymbol{J}(\boldsymbol{u}), \tag{2}$$

where $U \subset \mathbb{R}^m$ denotes the feasible input set.

Remark 1. The cost function $\boldsymbol{J}(\cdot)$ considered in this work is MIMO, unknown, and differentiable. Each component of $\boldsymbol{J}(\cdot)$ may possess multiple local minima, local maxima, and saddle points. This setting is significantly weaker than those commonly adopted in the existing ESC literature. For instance, many ESC results, such as [5, Assumption 3], require the existence of a unique local or global optimum. In contrast, the present work imposes no such requirement. Consequently, the resulting optimization problem is highly challenging due to the simultaneous presence of an unknown MIMO cost function, multiple critical points, and high-dimensional decision variables.

Motivated by this challenge, we impose a mild growth condition on the cost function.

Assumption 1. Function $\boldsymbol{J}(\cdot)$ is continuously differentiable, and there exists a constant $\mu > 0$ such that

$$\|\boldsymbol{J}(\boldsymbol{u})\| = O(\|\boldsymbol{u}\|^\mu) \quad \text{as } \|\boldsymbol{u}\| \to \infty, \tag{3}$$

where μ is assumed to be known. Here, $O(\|\boldsymbol{u}\|^\mu)$ denotes the order of $\|\boldsymbol{u}\|^\mu$ [13, Definition 10.1], and $\|\cdot\|$ is the standard Euclidean norm.

Remark 2. Condition (3) ensures that the growth of $\boldsymbol{J}(\boldsymbol{u})$ with respect to $\|\boldsymbol{u}\|$ is at most polynomial. This excludes functions that grow too rapidly (e.g. exponential, factorial, or super-exponential), while encompassing most cost functions commonly used in optimization, control, and machine learning, particularly those arising from physical systems or quadratic penalties. Although the exact value of μ may not be available in practice, it can be reasonably estimated, and such an estimate can be used without affecting the applicability of the proposed algorithm.

However, due to the existence of sensor dynamics, the measured cost function $\boldsymbol{J}(\boldsymbol{u}_k)$ is used to drive the following discrete-time MISO LTI system:

$$\begin{cases} \boldsymbol{x}_k = A\boldsymbol{x}_{k-1} + B\boldsymbol{v}_{k-1}, \quad \boldsymbol{x}_0 \in \mathbb{R}^n, \\ y_k = C\boldsymbol{x}_k, \end{cases} \tag{4}$$

where $\boldsymbol{x}_k \in \mathbb{R}^n$ and $y_k \in \mathbb{R}$ denote the state and output of the linear subsystem, respectively, and A, B, C are matrices of compatible dimensions. The block diagram of the MISO Hammerstein system considered in this paper is shown in Fig. 1.

Remark 3. The MISO Hammerstein model with an associated cost function naturally represents many real engineering systems where multiple inputs influence a vector-valued performance index that is observed indirectly through unknown linear dynamics and static nonlinearities. For instance, consider a small-scale chemical reactor with three actuated inputs: feed rate, temperature, and catalyst concentration. The performance index may include multiple outputs such as product concentration, reaction selectivity, and energy consumption. These outputs are measured through sensors with their own dynamic behavior, such as delays, filtering, or amplification, which means the observed cost function differs from the underlying true performance. We will show that such a setting is highly challenging in Remark 4, where a simple illustrative example demonstrates how the combination of a multi-input cost function and linear dynamics can transform a straightforward minimum into a saddle point, highlighting the difficulty of ESC in practical engineering systems.

Although matrices A, B, and C are unknown, it is assumed that this discrete-time LTI system satisfies the following assumption, which is widely used in ESC for dynamic systems, for example, [5, Assumption 2].

Assumption 2. Matrix A is stable, i.e.

$$\rho(A) := \max_{1\le i\le n} |\lambda_i| < 1, \tag{5}$$

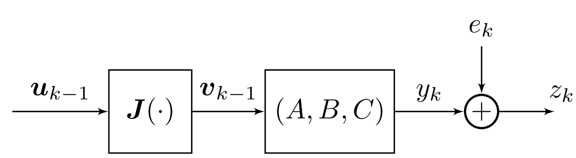

Fig. 1. A MISO Hammerstein system.

where λ_i is a root of the characteristic polynomial $p(\lambda) = \det(\lambda I - A)$ with $|\lambda_i|$ its modulus, and I denotes the identity matrix.

As matrix A is stable, the matrix $I - A$ is nonsingular. This implies that the mapping from the input to the steady-state output becomes

$$y_{\text{ss}}(\boldsymbol{v}) = C(I - A)^{-1} B\boldsymbol{v},$$

with the following input to steady-state output cost function:

$$Q(\boldsymbol{u}) = G\boldsymbol{J}(\boldsymbol{u}) = \sum_{i=1}^{l} g_i \boldsymbol{J}_i(\boldsymbol{u}), \tag{6}$$

where $G = [g_1, \dots, g_l] := C(I - A)^{-1}B$.

Note that the weight vector G can have positive or negative entries: positive values indicate minimization of the corresponding objective, while negative values indicate maximization. Thus, $Q(\boldsymbol{u})$ represents a scalarized cost for a *mixed minimization–maximization* problem rather than a conventional multi-objective weighted sum.

Recall that a *Pareto solution* to the multi-objective optimization problem (2) refers to a feasible input for which no objective can be improved without degrading at least one other objective, whereas a *scalarized* $(weighted)$ *Pareto solution* is obtained by minimizing a weighted sum of the objectives. For a differentiable unconstrained multi-objective problem, a *Pareto stationary point* is a stationary point of some positively weighted scalarized optimization problem.

Remark 4. The introduction of the linear dynamics can fundamentally alter the observed input-to-steady-state-output cost $Q(\cdot)$, defined in (6), potentially transforming an original minimum of $\boldsymbol{J}(\boldsymbol{u})$ into a saddle point.

For example, consider a three-input, two-output cost function

$$\boldsymbol{J}(\boldsymbol{u}) = \begin{bmatrix} u_1^2 + u_2^2 \\ u_2^2 + u_3^2 \\ u_1^2 + u_3^2 \end{bmatrix}, \quad \boldsymbol{u} \in \mathbb{R}^3,$$

which is strictly convex in all inputs. Each component of $\boldsymbol{J}$ has a unique global minimum at

$$\boldsymbol{u}^* = [0, 0, 0]^\top.$$

Now consider a linear system with

$$A = \begin{bmatrix} 0.5 & 0 \\ 0 & 0.5 \end{bmatrix}, \quad B = \begin{bmatrix} 1 & 1 & 0 \\ 0 & 1 & 1 \end{bmatrix},$$

and various configurations of the observation matrix C.

When $C = [-1, 2]$, the observed scalar cost is

$$Q(\boldsymbol{u}) = C(I - A)^{-1}B\,\boldsymbol{J}(\boldsymbol{u}) = 2u_1^2 + 6u_3^2,$$

so the original minimum property of $\boldsymbol{J}(\boldsymbol{u})$ is preserved. However, when $C = [1, -2]$, $Q(\boldsymbol{u}) = -2u_1^2 - 6u_3^2$ transforms the original minimum of $\boldsymbol{J}(\boldsymbol{u})$ into a maximum point in $Q(\boldsymbol{u})$. Furthermore, when $C = [3, -2]$, then $Q(\boldsymbol{u}) = 2u_1^2 + 8u_2^2 - 2u_3^2$. In this case, the Hessian of $Q(\boldsymbol{u})$ at $\boldsymbol{u}^*$ is $H_Q = \text{diag}(4, 16, -4)$, which has mixed signs. Consequently, the original minimum of $\boldsymbol{J}(\boldsymbol{u})$ is mapped to a saddle point in $Q(\boldsymbol{u})$. This illustrates that the linear dynamics can fundamentally alter both the location and nature of the extrema of $\boldsymbol{J}(\cdot)$, making the design of ESC nontrivial.

We define the set of critical points of ∇Q

$$U^* = \{\boldsymbol{u} \in \mathbb{R}^m : \nabla \boldsymbol{J}(\boldsymbol{u}) B^\top (I - A)^{-\top} C^\top = 0\}, \tag{7}$$

as according to Assumption 1, $Q(\cdot)$ is differentiable, where $\nabla \boldsymbol{J}(\boldsymbol{u}) = [\boldsymbol{J}'(\boldsymbol{u})]^\top$, the transpose of the Jacobian of $\boldsymbol{J}(\boldsymbol{u})$. We also define the distance to this set as $d(\boldsymbol{u}, U^*) := \inf_{\boldsymbol{v} \in U^*} \|\boldsymbol{u} - \boldsymbol{v}\|$ the distance from $\boldsymbol{u}$ to the set U^*.

Since the cost function Q is unknown, possibly high-dimensional, and may have multiple critical points, we need to assume not only that the optimal set U^* is nonempty, but also the existence of a guiding function that ensures that ESC can systematically make progress toward U^*.

Assumption 3. The optimal solution set U^{**} of the cost function $Q : \mathbb{R}^m \to \mathbb{R}$ is nonempty, i.e.

$$U^{**} := \left\{ \boldsymbol{u} \in \mathbb{R}^m : Q(\boldsymbol{u}) = \min_{\boldsymbol{v} \in \mathbb{R}^m} Q(\boldsymbol{v}) =: Q^* \right\} \neq \emptyset.$$

Moreover, there exists a continuously differentiable function $V : \mathbb{R}^m \to \mathbb{R}$ such that

$$\inf_{\delta \le d(\boldsymbol{u}, U^*) \le \Delta} \nabla V(\boldsymbol{u})^\top \nabla Q(\boldsymbol{u}) > 0 \tag{8}$$

for any $0 < \delta < \Delta$, where $d(\boldsymbol{u}, U^*)$ denotes the distance from $\boldsymbol{u}$ to the set U^*. Furthermore, the set $V(U^*) := \{V(\boldsymbol{u}) : \boldsymbol{u} \in U^*\}$ is nowhere dense.

Remark 5. Assumption 3 has two components. The first ensures that the cost function has at least one optimal input, which is a basic feasibility requirement for any optimization problem. A natural necessary condition for this assumption to hold is that not all components of G are zero simultaneously. The second provides a Lyapunov-like function $V(\boldsymbol{u})$ to guide iterative algorithms toward the optimal set U^*. Specifically, the gradient alignment condition guarantees that when the current input $\boldsymbol{u}$ is not too close to U^* (i.e. $\delta \le d(\boldsymbol{u}, U^*) \le \Delta$), the gradient of V points in a direction that reduces $Q(\boldsymbol{u})$, ensuring systematic progress toward the optimum. The requirement that $V(U^*)$ is nowhere dense avoids pathological cases where V could be constant over a large subset of U^*, which could stall convergence. Together, these conditions provide a mathematically tractable way to ensure convergence of the ESC algorithm, even when the cost function is unknown, multi-dimensional, and nonconvex.

2.2. *ESC for MISO Hammerstein systems*

Control objective: The goal of this work is to design an ESC algorithm that converges to the set U^*, which consists of all stationary points of the composite MIMO cost function $Q(\cdot)$ defined in (6) under Assumptions 1–3.

Remark 6. Achieving this control objective is highly challenging due to the unknown MIMO cost function, multiple local extrema, saddle points, and unmodeled system dynamics, as discussed in Remark 4. Despite these challenges, convergence to stationary points remains practically meaningful in many engineering applications, as these points often correspond to safe, feasible, and predictable operating regimes.

It is worthwhile to emphasize that the scalar objective arises from the steady-state input–output relation of the LTI sensor subsystem, and the vector G is not chosen as a design weight but is determined by the system structure. Consequently, the ESC algorithm optimizes a system-induced scalar performance index, which represents a prescribed trade-off among the objectives rather than an exploration of the Pareto front. The control objective is relatively weak, since the ESC algorithm may converge to any stationary point — including a local maximum, minimum, or saddle point. In many engineering systems, stronger assumptions can be satisfied. For example, under the following assumption, stronger convergence results can be established.

Assumption 4. The vector $C(I-A)^{-1}B$ is positive, where a vector is said to be positive if each of its elements is strictly positive.

Remark 7. Assumption 4 requires knowledge of the sign of the control gain. It is worth noting that this assumption is not restrictive in practice, as engineers typically obtain such information through experimental testing during system commissioning or identification. For example, this can be determined experimentally without requiring an explicit plant model. Specifically, a small constant perturbation $\Delta u > 0$ is applied around a steady operating point, and the corresponding steady-state output variation Δy is measured after transients have decayed. The sign of the control gain is then given by sign$(\Delta y/\Delta u)$. If $\Delta y > 0$, the system is direct-acting (positive control gain); otherwise, it is reverse-acting (negative control gain). This procedure relies only on local steady-state behavior and is therefore applicable to general stable LTI systems operating in a neighborhood of the equilibrium. Under this assumption, significantly stronger convergence results can be established.

Under Assumption 4, i.e. when the subsystem-induced weight vector $G = C(I-A)^{-1}B$ satisfies $G_i > 0$ for all components, the solution $\boldsymbol{u}_{\text{ss}}^*$ of the scalarized cost

$$Q(\boldsymbol{u}) = G\,\boldsymbol{J}(\boldsymbol{u})$$

is a *parameterized Pareto solution* of the multi-objective cost function $\boldsymbol{J}(\cdot)$. Since the weight vector G is determined by the LTI subsystem, $\boldsymbol{u}_{\text{ss}}^*$ corresponds to a specific point on the Pareto front, rather than being freely selectable.

Under the additional Assumption 4, we can obtain sharper convergence results than those in Theorem 1, as presented in Corollary 2.

To summarize, the ESC for Hammerstein systems targets a directionally weighted scalarized steady-state optimum defined by the linear subsystem. This optimum is generally not Pareto optimal unless a positive weight $G > 0$ is imposed, under which convergence to a Pareto optimal solution is guaranteed.

3. ESC Using Random Perturbations

This work proposes a random-perturbation-based ESC, as illustrated in Fig. 2, which is motivated by the randomized gradient-free methods in [14, 15].

We consider a randomized approximation of the objective function Q

$$\begin{aligned} Q_\alpha(\boldsymbol{u}) &:= \mathrm{E}_{\boldsymbol{W}}[Q(\boldsymbol{u}+\alpha\boldsymbol{W})] \\ &= \int_{\mathbb{R}^m} Q(\boldsymbol{u}+\alpha\boldsymbol{w})p(\boldsymbol{w})\mathrm{d}\boldsymbol{w}, \end{aligned} \tag{9}$$

where $p(\cdot)$ is the probability density function of random vector $\boldsymbol{W}$, and $\alpha > 0$ is a smoothing parameter.

It can be shown, referring to [14, 15], that if $\boldsymbol{W} \sim \mathcal{U}(\mathcal{B})$ is uniformly distributed over $\mathcal{B} := \{\boldsymbol{u} \in \mathbb{R}^m : \|\boldsymbol{u}\| \le 1\}$ — the unit ball centered at the origin in $\mathbb{R}^m$ — then the gradient of $Q_\alpha(\boldsymbol{u})$ is given by

$$\nabla Q_\alpha(\boldsymbol{u}) = \frac{m}{\alpha}\mathrm{E}_{\boldsymbol{V}\sim\mathcal{U}(\partial\mathcal{B})}\left[Q(\boldsymbol{u}+\alpha\boldsymbol{V})\boldsymbol{V}\right]. \tag{10}$$

If $\boldsymbol{W} \sim \mathcal{N}(0, I)$ is a standard normal random vector, then

$$\begin{aligned} \nabla Q_\alpha(\boldsymbol{u}) &= \frac{1}{\alpha}\mathrm{E}_{\boldsymbol{W}}[Q(\boldsymbol{u}+\alpha\boldsymbol{W})\boldsymbol{W}] \\ &= \frac{1}{\alpha}\int_{\mathbb{R}^m} Q(\boldsymbol{u}+\alpha\boldsymbol{w})\boldsymbol{w}p(\boldsymbol{w})\mathrm{d}\boldsymbol{w}. \end{aligned} \tag{11}$$

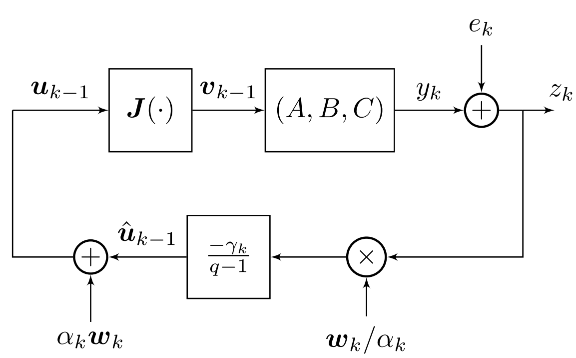

Fig. 2. ESC with random perturbations for MISO Hammerstein systems.

This motivates the ESC algorithm for optimizing the Hammerstein system, as shown in Fig. 2.

Since $Q(\cdot)$ is unknown and the observed output is perturbed by e_k, even when a constant input $\boldsymbol{u}_k \equiv \boldsymbol{u}$ is applied, the exact function value $Q(\boldsymbol{u})$ cannot be determined. Consequently, the optimization problem must be solved in real time by utilizing the system input $\boldsymbol{u}_k$ and the perturbed output z_k.

3.1. *ESC using stochastic approximation*

For a selected initial value $\hat{\boldsymbol{u}}_0$, the following stochastic approximation-based ESC takes the following form:

$$z_k = y_k + e_k, \tag{12}$$

$$\boldsymbol{u}_{k-1} = \hat{\boldsymbol{u}}_{k-1} + \alpha_k \boldsymbol{w}_k, \tag{13}$$

$$\hat{\boldsymbol{u}}_k = \begin{cases} \hat{\boldsymbol{u}}_{k-1} - \gamma_k m z_k \boldsymbol{w}_k/\alpha_k & \text{if } \boldsymbol{w}_k \sim \mathcal{U}(\partial\mathcal{B}); \\ \hat{\boldsymbol{u}}_{k-1} - \gamma_k z_k \boldsymbol{w}_k/\alpha_k & \text{if } \boldsymbol{w}_k \sim \mathcal{N}(0, I), \end{cases} \tag{14}$$

where $\{\alpha_k\}_{k\geq 1} \in \mathbb{R}$ is a sequence of smoothing parameters, $\{\gamma_k\}_{k\geq 1} \in \mathbb{R}$ is a sequence of step-sizes, and $\{\boldsymbol{w}_k\}_{k\geq 1} \in \mathbb{R}^m$ is a sequence of random perturbations and $\{e_k\}_{k\geq 1}$ is a sequence of observation noises.

The following conditions are used to design sequences: $\{\alpha_k\}_{k\geq 1}$, $\{\gamma_k\}_{k\geq 1}$, $\{e_k\}_{k\geq 1}$, and $\{\boldsymbol{w}_k\}_{k\geq 1}$.

Condition 1. The random sequence $\{\boldsymbol{w}_k\}_{k\geq 1}$ is an independent and identically distributed (i.i.d.) sequence of random perturbations: $\boldsymbol{w}_k \sim \mathcal{U}(\partial\mathcal{B})$ or $\boldsymbol{w}_k \sim \mathcal{N}(0, I)$.

Condition 2. The sequences $\{\gamma_k\}_{k\geq 1}$ and $\{\alpha_k\}_{k\geq 1}$ are chosen as

$$\gamma_k = \frac{1}{k}, \quad \alpha_k = \frac{\alpha_0}{k^\alpha} \quad \text{with } \alpha < \frac{1}{1+\mu} \text{ and } \alpha_0 > 0.$$

Remark 8. The step-size sequence $\gamma_k = 1/k$ is commonly used in stochastic approximation algorithms to guarantee diminishing updates while ensuring convergence. This choice also establishes a discrete-time scale separation between the fast process driven by γ_k and the slower adaptation governed by α_k, satisfying the standard two-time-scale stochastic approximation condition $\gamma_k/\alpha_k \to 0$ as $k \to \infty$. As noted in [5], such a time-scale separation is necessary for applying ESC (i.e. the solution of an optimization problem) to a dynamic system.

Regarding the noise random process $\{e_k\}$, a classical assumption is as follows.

Condition 3. $\{e_k\}_{k\geq 1}$ is an i.i.d. sequence such that $\mathrm{E}[e_k^2] < \infty$ and e_k is independent of $\{\boldsymbol{w}_i : 1 \leq i \leq k\}$.

It is noted that such a signal originates from measurement noises, which usually satisfy this condition. The random process $\{e_k\}$ provides an additional design degree of freedom. Complementing the original observation noise $\{e_k^{(1)}\}$, we can appropriately construct perturbation signal $\{e_k^{(2)}\}$ such that the combined excitation signal $e_k = e_k^{(1)} + e_k^{(2)}$ satisfies Condition 4 stated below, thereby making the proposed algorithm more robust to a broad class of noises.

It is worth noting that this choice of random perturbations is motivated by the randomized gradient-free methods in [14,15]. However, the proposed approach can be extended to accommodate other types of random perturbations as well.

Note that the ESC (13) and (14) can be rewritten as

$$\begin{aligned} \hat{\boldsymbol{u}}_k &= \hat{\boldsymbol{u}}_{k-1} - \gamma_k[y_k + e_k]\boldsymbol{w}_k/\alpha_k \\ &= \hat{\boldsymbol{u}}_{k-1} - \gamma_k(\tilde{\nabla} Q(\hat{\boldsymbol{u}}_{k-1}) + \boldsymbol{\xi}_k' + \boldsymbol{\eta}_k), \end{aligned} \tag{15}$$

where

$$\tilde{\nabla} Q(\hat{\boldsymbol{u}}_{k-1}) = Q(\hat{\boldsymbol{u}}_{k-1} + \alpha_k \boldsymbol{w}_k)\boldsymbol{w}_k/\alpha_k \tag{16}$$

is an estimate of the gradient of Q at $\hat{\boldsymbol{u}}_{k-1}$ with the perturbation e_k

$$\boldsymbol{\xi}_k' = [y_k - Q(\hat{\boldsymbol{u}}_{k-1} + \alpha_k \boldsymbol{w}_k)]\boldsymbol{w}_k/\alpha_k, \tag{17}$$

$$\boldsymbol{\eta}_k = e_k \boldsymbol{w}_k/\alpha_k. \tag{18}$$

The above formulation shows that the ESC algorithm (13) and (14) with random perturbations can be interpreted as a randomized *zeroth-order optimization* method.

Remark 9. The SA ESC algorithm can be extended and adapted in practical scenarios as follows:

(1) **Input constraints.** When the input is restricted to a set $U \subset \mathbb{R}^m$, the projected SA ESC algorithm should be used. This is achieved by replacing (14) with

$$\hat{\boldsymbol{u}}_k = \begin{cases} \Pi_U(\hat{\boldsymbol{u}}_{k-1} - \gamma_k\, m\, z_k \boldsymbol{w}_k/\alpha_k) & \text{if } \boldsymbol{w}_k \sim \mathcal{U}(\partial\mathcal{B}), \\ \Pi_U(\hat{\boldsymbol{u}}_{k-1} - \gamma_k\, z_k \boldsymbol{w}_k/\alpha_k) & \text{if } \boldsymbol{w}_k \sim \mathcal{N}(0, I), \end{cases} \tag{19}$$

where $\Pi_U(\cdot)$ denotes the Euclidean projection onto U.

(2) **Extension to MISO Hammerstein–Wiener systems.** The ESC algorithm (13) and (14) can be applied to the MISO Hammerstein–Wiener system in Fig. 3. The modification lies in the output observation equation, which becomes

$$z_k = h(\boldsymbol{y}_k) + e_k, \tag{20}$$

where $\boldsymbol{y}_k \in \mathbb{R}^r$ and $h : \mathbb{R}^r \to \mathbb{R}$ is a static nonlinear function satisfying appropriate smoothness conditions,

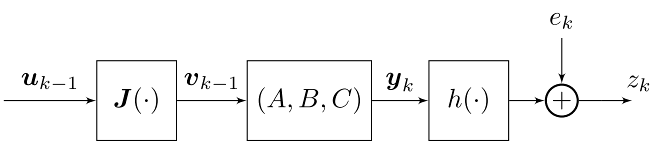

Fig. 3. A MISO Hammerstein–Wiener system.

ensuring that assumptions analogous to Assumption 3 hold.

Since normal random variables can take arbitrarily large values, though with very low probability, applying them to a nonflat cost function $\boldsymbol{J}(\cdot)$ may produce input changes that possibly make the system unstable. In practice, this means that the output y_k could grow without bound, causing the controller to fail. To prevent this, we introduce an adaptive version of the algorithm in the following section that keeps the inputs and outputs within safe limits.

3.2. *Stochastic approximation algorithm with expanding truncations*

Let $\{M_k\}$ be a sequence of positive numbers that diverges to infinity, and let $\boldsymbol{u}^0 \in \mathbb{R}^m$ be a constant reference point. Vector $\boldsymbol{u}^0$ serves as a reset to prevent the iterates from diverging when trial updates exceed the allowable range. Its choice is flexible, but it is typically selected near the expected operating region to avoid abrupt jumps. As the truncation bounds M_k grow, the effect of resets diminishes, allowing the algorithm to safely explore the input space while maintaining stability. Variable σ_k counts the number of truncations up to time k.

Given an initial estimate $\hat{\boldsymbol{u}}_0$, the SAAWET ESC algorithm for the MISO Hammerstein system (1), (4), and (12) recursively generates sequences $(\hat{\boldsymbol{u}}_k, \sigma_k)$ as follows. At each iteration $k \geq 1$, a trial update is computed by

$$\tilde{\boldsymbol{u}}_k = \begin{cases} \hat{\boldsymbol{u}}_{k-1} - \dfrac{\gamma_k m z_k \boldsymbol{w}_k}{\alpha_k} & \text{if } \boldsymbol{w}_k \sim \mathcal{U}(\partial\mathcal{B}); \\ \hat{\boldsymbol{u}}_{k-1} - \dfrac{\gamma_k z_k \boldsymbol{w}_k}{\alpha_k} & \text{if } \boldsymbol{w}_k \sim \mathcal{N}(0, I). \end{cases} \tag{21}$$

The next iterate $\hat{\boldsymbol{u}}_k$ is then obtained by applying the truncation rule:

$$\hat{\boldsymbol{u}}_k = \tilde{\boldsymbol{u}}_k 1_{\{\|\tilde{\boldsymbol{u}}_k\| \leq M_{\sigma_{k-1}}\}} + \boldsymbol{u}^0 1_{\{\|\tilde{\boldsymbol{u}}_k\| > M_{\sigma_{k-1}}\}}, \tag{22}$$

$$\sigma_k = \sum_{i=1}^{k} 1_{\{\|\tilde{\boldsymbol{u}}_i\| > M_{\sigma_{i-1}}\}}, \quad \sigma_0 = 0, \tag{23}$$

where 1_A is the indicator function of event A meaning it equals 1 if A occurs and 0 otherwise. This truncation ensures that

$$\|\hat{\boldsymbol{u}}_k\| \leq M_{\sigma_k}, \quad \forall\, k \geq 0,$$

so that the iterates remain bounded at every step.

The SAAWET ESC algorithm adaptively searches for a stationary point of Q: if the trial update $\tilde{\boldsymbol{u}}_k$ exceeds the current truncation bound $M_{\sigma_{k-1}}$, the algorithm resets $\hat{\boldsymbol{u}}_k$ to $\boldsymbol{u}^0$ and increments the truncation threshold to M_{σ_k}.

Remark 10. The SAAWET ESC algorithm (21)–(23) has two key features that contribute to its robustness and flexibility:

(1) **Use of the reset point $\boldsymbol{u}^0$.** The reset point can be interpreted as prior knowledge of the problem's optimal solution. In practice, it can be chosen randomly from a set of candidate solutions. The closer these candidates are to the true optimum, the higher the likelihood of convergence to the global optimum. This property makes the algorithm suitable for nonconvex optimization problems, while still ensuring asymptotic convergence regardless of the initial choice.
(2) **Role of the truncation sequence M_k.** The sequence M_k is crucial for controlling the propagation of uncertainty caused by observation noise and stochastic perturbations through the nonlinear mapping $\boldsymbol{J}$ and the linear system. Appropriate growth bounds prevent divergence: typically, $M_k = O(k^{1/(1+\mu)})$ for uniform perturbations and $M_k = O(\ln k)$ for normal perturbations. This design ensures both stability and reliable convergence of the algorithm.

Condition 4. For any sufficiently large integer N, the following condition holds:

$$\lim_{T \to 0} \limsup_{k \to \infty} \frac{1}{T} \left\| \sum_{i=n_k}^{m(n_k, T)} \frac{\gamma_i e_i \boldsymbol{w}_i}{\alpha_i} 1_{\{\|\hat{\boldsymbol{u}}_{i-1}\| \leq N\}} \right\| = 0$$

for any $\{n_k\}$ such that $\hat{\boldsymbol{u}}_{n_k - 1}$ converges, where

$$m(k, t) := \max \left\{ m : \sum_{i=k}^{m} \gamma_i \leq t \right\}. \tag{24}$$

Remark 11. Condition 4 regarding e_k is quite general, allowing state-dependent noise, thereby facilitation algorithm design and theoretical analysis. It holds if

$$\sum_{k=1}^{\infty} \frac{\gamma_k e_k \boldsymbol{w}_k}{\alpha_k} < \infty \quad \text{a.s.}$$

which is satisfied if

$$\sum_{k=1}^{\infty} \gamma_k^2 / \alpha_k^2 < \infty \tag{25}$$

and $\{e_k\}$ satisfies Condition 3.

Finally, for $k \geq 1$, $\hat{\boldsymbol{u}}_k$ is measurable with respect to the σ-algebra

$$\mathscr{F}_k = \sigma(\hat{\boldsymbol{u}}_0, e_i, \boldsymbol{w}_i : 1 \leq i \leq k), \tag{26}$$

generated by the history of the random variables up to time k.

4. Convergence Analysis

In this section, we present an analysis of almost sure convergence for the SAAWET-based ESC (21)–(23) applied to the MISO Hammerstein system (1), (4), and (12).

The primary result regarding almost sure convergence of the SAAWET ESC algorithm (21)–(23) is stated below. The theorem indicates that with appropriately selected sequences of step-sizes and smoothing parameters, the estimates $\hat{u}_k$ generated by the algorithm converge to the set of optimal solutions of $\min_{u\in\mathbb{R}^m} Q(u)$ with probability 1.

Theorem 1. *Assume that Assumptions* 1–3 *hold. Set* $M_k = k^{1/(1+\mu)}$ *for uniformly distributed perturbations and* $M_k = \ln k$ *for normally distributed ones. Assume that the random sequences* $\{\alpha_k\}_{k\geq 1}$, $\{\gamma_k\}_{k\geq 1}$, $\{e_k\}_{k\geq 1}$, *and* $\{\boldsymbol{w}_k\}_{k\geq 1}$ *satisfy Conditions* 1, 2, *and* 4*. Let* $\{\hat{\boldsymbol{u}}_k\}_{k\geq 0}$ *be the iterates generated by the SAAWET ESC algorithm* (21)–(23) *for the MISO Hammerstein system* (1), (4), *and* (12)*. Vector* $\boldsymbol{u}^0$ *used in* (22) *is selected such that* $V(\boldsymbol{u}^0) < \inf_{\|\boldsymbol{u}\|=c_0} V(\boldsymbol{u})$ *for some* $c_0 > 0$ *and* $\|\boldsymbol{u}^0\| < c_0$*. Then the algorithm yields almost sure convergence to the set of optimal solutions*:

$$\lim_{k\to\infty} d(\hat{\boldsymbol{u}}_k, U^*) = 0 \quad \textit{a.s.}$$

Proof. We rewrite the trial step (21) as

$$\tilde{\boldsymbol{u}}_k = \hat{\boldsymbol{u}}_{k-1} - \gamma_k(\nabla Q(\hat{\boldsymbol{u}}_{k-1}) + \boldsymbol{\xi}_k + \boldsymbol{\eta}_k), \tag{27}$$

where $\boldsymbol{\xi}_k = \boldsymbol{\xi}_k^{(1)} + \boldsymbol{\xi}_k^{(2)} + \boldsymbol{\xi}_k^{(3)}$ with

$$\boldsymbol{\xi}_k^{(1)} = \mathrm{E}[\tilde{\nabla} Q(\hat{\boldsymbol{u}}_{k-1})|\mathscr{F}_{k-1}] - \nabla Q(\hat{\boldsymbol{u}}_{k-1}), \tag{28}$$

$$\boldsymbol{\xi}_k^{(2)} = \tilde{\nabla} Q(\hat{\boldsymbol{u}}_{k-1}) - \mathrm{E}[\tilde{\nabla} Q(\hat{\boldsymbol{u}}_{k-1})|\mathscr{F}_{k-1}], \tag{29}$$

$$\boldsymbol{\xi}_k^{(3)} = y_k \boldsymbol{w}_k/\alpha_k - \tilde{\nabla} Q(\hat{\boldsymbol{u}}_{k-1}), \tag{30}$$

and $\tilde{\nabla} Q(\hat{\boldsymbol{u}}_{k-1})$, $\boldsymbol{\eta}_k$ are defined as (16) and (18), respectively. Consequently, the algorithm (21)–(23) presents an SAAWET with regression function $\nabla Q(\cdot)$ and observation noise $\boldsymbol{\xi}_k + \boldsymbol{\eta}_k$. Here $\mathscr{F}_k$ is defined in (26).

To prove the almost sure convergence of $\hat{\boldsymbol{u}}_k$ to the root set U^* of the regression function $\nabla Q(\cdot)$, we apply the general convergence theorem given in [16, Theorem 2.2.1]. It is evident that the step-size condition [16, A2.2.1] is automatically satisfied. The Lyapunov condition [16, A2.2.2], along with the condition [16, A2.2.4] regarding the regression function, had been fulfilled by Assumption 3. Therefore, it suffices to verify the noise condition

$$\lim_{T\to 0} \limsup_{k\to\infty} \frac{1}{T} \left\| \sum_{i=n_k}^{m(n_k,T)} \gamma_i \boldsymbol{\xi}_i^{(\ell)} \right\| = 0, \ell = 1, 2, 3 \tag{31}$$

for any $\{n_k\}$ such that $\hat{\boldsymbol{u}}_{n_k-1}$ converges.

We note that if the term $\boldsymbol{\xi}_k^{(3)}$ vanishes, the algorithm (21)–(23) is consistent with the SAAWET optimizing the static function Q using the normal randomized gradient-free method. Therefore, the analysis of the noises $\boldsymbol{\xi}_k^{(1)}, \boldsymbol{\xi}_k^{(2)}$ is analogous to that presented in [17]. The challenge arises in the analysis of noise $\boldsymbol{\xi}_k^{(3)}$. The relevant lemmas and their proofs regarding noise analysis (31) are provided in the appendix. □

Remark 12. As the proposed algorithm is stochastic, its convergence analysis does not rely on the classical averaging arguments commonly used in deterministic dither-based ESC schemes. In deterministic periodic perturbation methods, convergence is typically established for the averaged system. Consequently, the actual closed-loop trajectories converge only to an $O(a)$ neighborhood of the optimizer, where a denotes the dither amplitude. In contrast, the stochastic nature of the proposed scheme enables the use of stochastic approximation techniques to analyze the true closed-loop system directly. As demonstrated in our simulation studies, the actual closed-loop trajectories converge to the true stationary set U^*, rather than to a neighborhood whose size depends on the perturbation magnitude.

For the complex Hammerstein system under a model-free ESC framework, where both the cost function and the LTI dynamics are unknown, achieving almost sure convergence to the set of critical points is already nearly the strongest theoretical guarantee under only Assumptions 1–3.

The following corollary shows that if the sign of the steady-state input–output gain of the LTI system is known (Assumption 4) and additional restrictions are imposed on the cost function, a sharper result can be established: the algorithm converges to the set of Pareto stationary points, or even a point in the Pareto optimal set.

Recall that an extended real-valued function $f : \mathbb{R}^m \to [-\infty, \infty]$ is called *proper* if its domain $\mathrm{dom}(f) := \{\boldsymbol{x} \in \mathbb{R}^m : f(\boldsymbol{x}) < \infty\}$ is nonempty. A proper function $f : \mathbb{R}^m \to [-\infty, \infty]$ is called *coercive* if

$$\lim_{\|\boldsymbol{x}\|\to\infty} f(\boldsymbol{x}) = \infty.$$

Let $L > 0$, a differentiable function $f : \mathbb{R}^m \to (-\infty, \infty]$ is said to be *L-smooth* if $\|\nabla f(\boldsymbol{x}) - \nabla f(\boldsymbol{y})\| \leq L\|\boldsymbol{x} - \boldsymbol{y}\|$ for all $\boldsymbol{x}, \boldsymbol{y} \in \mathbb{R}^m$. A differentiable function $f : \mathbb{R}^m \to \mathbb{R}$ is said to be *pseudo-convex* if for all $\boldsymbol{x}, \boldsymbol{y} \in \mathbb{R}^m$,

$$\nabla f(\boldsymbol{x})^\top (\boldsymbol{y} - \boldsymbol{x}) \geq 0 \Rightarrow f(\boldsymbol{y}) \geq f(\boldsymbol{x}).$$

Corollary 2. *Let Assumptions* 1, 2, *and* 4 *hold. Assume that* $U^{**} \neq \emptyset$ *and that* Q *is proper*, *coercive, and* L*-smooth. Then*, *the SAAWET ESC algorithm* (21)–(23) *converges almost surely to the set of Pareto stationary points with the weight defined in* (6), *and converges almost surely to a Pareto optimal solution if*, *furthermore*, Q *is pseudo-convex.*

Proof. By choosing Lyapunov functions $V(\boldsymbol{u}) = Q(\boldsymbol{u}) - Q^*$ and $V(\boldsymbol{u}) = \|\boldsymbol{u} - \boldsymbol{u}^\star\|^2$ (where $\boldsymbol{u}^\star \in U^*$ is arbitrary) respectively, it can be verified that all conditions of Theorem 1 are satisfied. Consequently, we have $\lim_{k\to\infty} d(\hat{\boldsymbol{u}}_k, U^*) = 0$ a.s., and no truncation occurs after a finite step $k_0 \geq 0$. This implies that the algorithm reduces to the Robbins–Monro iteration given in (27) for all $k \geq k_0$. Moreover, the noise term $\boldsymbol{\xi}_k$ can be decomposed into the form shown in (28)–(30). Notably, by leveraging the conclusions of Theorem 1 and following the standard stochastic approximation analysis framework for stochastic gradient descent-type algorithms, this corollary can be rigorously derived. □

Corollary 3. *Under the assumptions of Theorem* 1, *and further assuming that* Q *is a strictly convex function* (*which implies that* U^* *consists of a singleton* $\boldsymbol{u}^*$), *then the SAAWET ESC algorithm* (21)–(23) *attains an exact almost sure convergence*: $\lim_{k\to\infty} \hat{\boldsymbol{u}}_k = \boldsymbol{u}^*$ *a.s.*

5. Simulations

To validate the effectiveness of the proposed algorithm, we begin with a simple SISO Hammerstein system governed by a static nonlinear function. This example serves three purposes. First, it demonstrates that the conventional stochastic approximation-based ESC algorithm (13) and (14) may diverge when applied to nonconvex functions without input constraints. Second, it verifies that the proposed SAAWET-based ESC algorithm (21)–(23) effectively prevents divergence by adaptively constraining the iterates within an expanding compact set. Third, it illustrates how the sign of the steady-state gain $c(1-a)^{-1}b$ determines whether the algorithm converges to a local minimum or a local maximum of the cost function. This simple case therefore provides an intuitive validation of the theoretical results established in the previous sections.

To further demonstrate the performance and robustness of the proposed SAAWET-based ESC algorithm in a multi-dimensional setting, we consider a MISO Hammerstein system with a two-dimensional input and a static nonlinear mapping defined by benchmark test functions, including the Himmelblau, Beale, Six-Hump Camel Back, and Rosenbrock functions. These examples confirm that the proposed SAAWET-based ESC can successfully converge to the set U^*, defined in (7), through appropriate selection of the random design sequences.

Finally, we apply the proposed SA-based ESC algorithm to the material balance control of a well-established continuous stirred-tank reactor (CSTR) model, motivated by practical engineering applications. This example serves two purposes. First, it demonstrates that the proposed algorithm performs effectively in an industrial setting. Second, it shows that the method can be extended to ESC of MISO Hammerstein–Wiener systems. A comparison with the classical ESC algorithm highlights the advantages of our approach over algorithms with semi-global convergence.

5.1. *A SISO Hammerstein example*

Consider a SISO Hammerstein system. A static nonlinear function $J_1(u) = u^3/3 - u$ is examined, as shown in Fig. 4. It can be verified that -1 is a local maximum and $+1$ is a local minimum. This function has no global maximum or minimum.

The linear dynamic system takes the following form:

$$\begin{aligned} x_k &= a x_{k-1} + b v_{k-1}, \\ y_k &= c x_k, \\ z_k &= y_k + e_k, \end{aligned} \tag{32}$$

where $a = -0.5$.

The random perturbation sequence $\{e_k\}$ is selected as an ARMA(2,1) process, that is, an auto-regressive moving average (ARMA) process with two auto-regressive terms and one moving-average term:

$$\begin{aligned} &e_k = 0.3e_{k-1} - 0.15e_{k-2} + \epsilon_k + 0.2\epsilon_{k-1}, \\ &\epsilon_k \overset{\text{i.i.d.}}{\sim} \mathcal{N}(0, 0.1). \end{aligned} \tag{33}$$

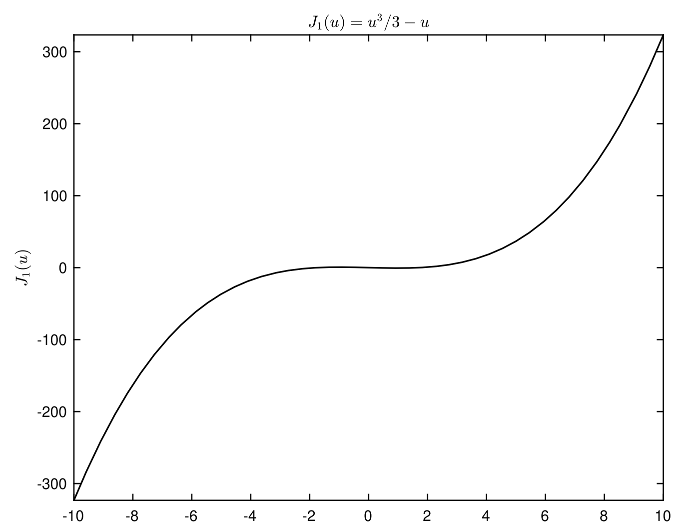

Fig. 4. The curve of function $J_1(\cdot)$.

For the SAAWET ESC algorithm (21)–(23), we use the initial value conditions $\hat{u}_0 = 5, x_0 = 0$, and the fixed point $u^0 = 0$. Set $M_k = 1 + k^{1/2}$ for uniformly distributed random perturbations and $M_k = \ln(k + 1)$ for normally distributed ones, the step-sizes $\gamma_k = 1/k$, and the smoothing parameters $\alpha_k = \alpha_0/k^{\alpha}$ with $\alpha_0 = 1.5$, and $\alpha = 0.25$.

We run the algorithms for $K = 500$ steps. We present the trajectories of the estimates $\hat{u}_k$ and outputs z_k versus the steps k in Figs. 5(a) and 5(b) under various scenarios, respectively. Note that in the graph legends, the labels "uniform" or "normal" indicate whether the dither w_k follows a uniform or normal distribution, and "with noise" or "without noise" denote whether the observed output e_k is used or not.

It can be observed that if $c(1-a)^{-1}b > 0$, the algorithm will seek the minimum of J, and if $c(1-a)^{-1}b < 0$, it will seek its maximum.

To verify the algorithm's robustness to initial conditions and compare the performance of different approaches, we evaluate the SAAWET ESC algorithm (21)–(23) (labeled as SAAWET-ESC) against the conventional SA ESC algorithm (13) and (14) (labeled as SA-ESC) and the adaptive gain ESC algorithm in [12] (labeled as adaptive gain ESC).

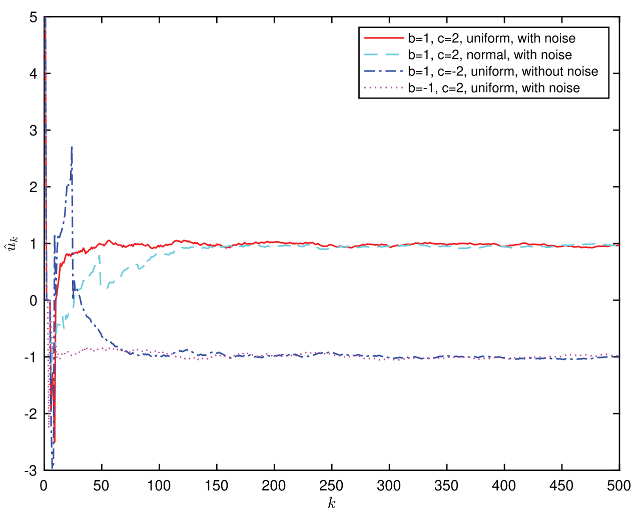

(a) Estimates $\hat{u}_k$ of the SAAWET ESC algorithm under different scenarios.

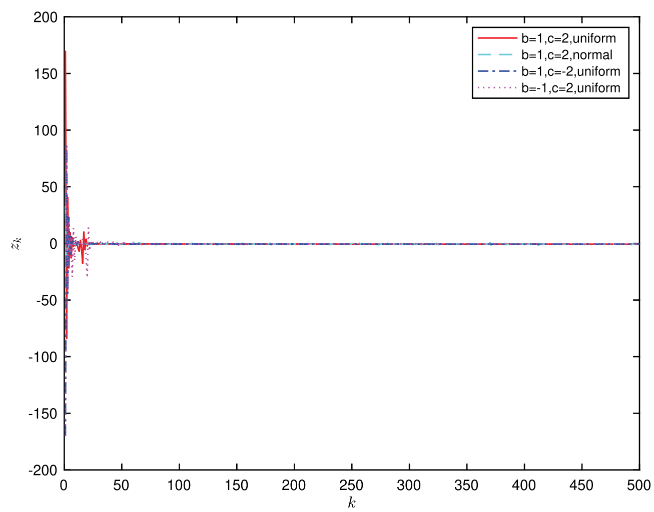

(b) Output z_k of the SISO Hammerstein system under different scenarios.

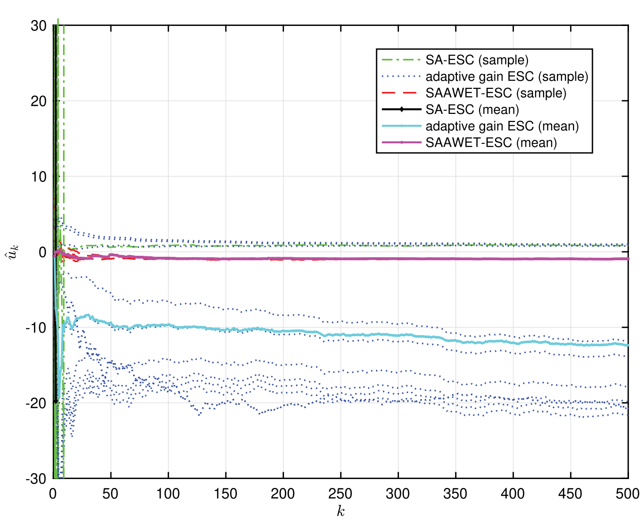

(c) Estimates $\hat{\boldsymbol{u}}_k$ of the compared algorithms with 10 random initial points.

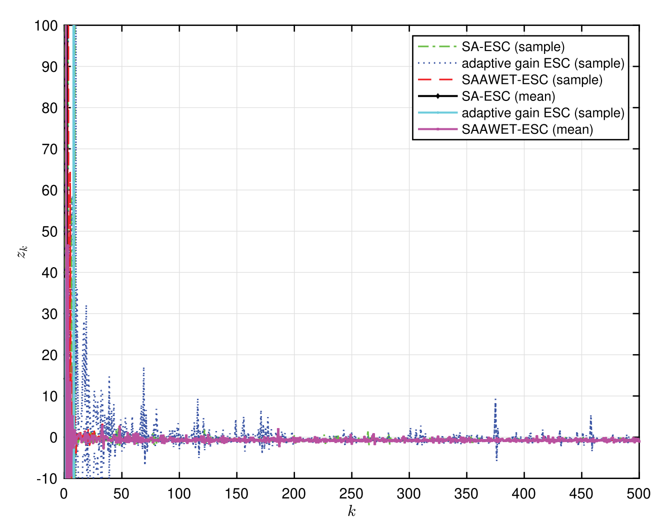

(d) Output z_k of the SISO Hammerstein system for the compared algorithms.

Fig. 5. Numerical experiments for the SISO Hammerstein system.

The SA ESC algorithm uses the same step-size and smoothing parameter sequences as the SAAWET-ESC algorithm, while the adaptive gain ESC algorithm employs $\epsilon_1 = 0.1$ and $\mu = 1$.

We randomly selected 10 initial values $\hat{u}_0$ within the range $[-10, 10]$ and conducted 10 independent experiments. In each experiment, perturbations were randomly drawn from uniform and normal distributions with equal probability, satisfying [12, Assumption A1]. The trajectories of $\hat{u}_k$ and z_k for each experiment are plotted in Figs. 5(c) and 5(d), respectively, together with the mean curve over the 10 experiments. For clarity, the range of $\hat{u}_k$ is limited to $[-30, 30]$ and that of z_k to $[-10, 100]$.

Note that the SA ESC algorithm without truncation or expanding truncation diverged in 9 out of 10 experiments, which is why some trajectories are omitted from the figures. To highlight the differences, the SAAWET-ESC algorithm uses $c = -2$, while all other parameters and linear system settings for the remaining algorithms are kept identical.

5.2. *A MISO Hammerstein example*

Consider a two-dimensional input MISO Hammerstein system with a static nonlinearity represented by one of the four test functions, as illustrated on Figs. 6(a) and 6(b), which display the corresponding surface and contour plots, respectively. These four benchmark cost functions are widely used in nonlinear optimization and control studies to evaluate the performance and robustness of search algorithms under different landscape conditions. Each function exhibits distinct structural properties, providing a diverse set of challenges for the proposed SAAWET-based ESC algorithm.

- **Himmelblau's function:**
$$J_H(u_1, u_2) = (u_1^2 + u_2 - 11)^2 + (u_1 + u_2^2 - 7)^2$$
is a multi-modal function possessing four identical local minima and one saddle point. Such a function is particularly suitable for examining whether the algorithm can identify one of several equivalent extrema in a nonconvex landscape. It has four identical local minima at
$$\begin{aligned} \boldsymbol{u}_1^* &= [3,\ 2]^\top, \\ \boldsymbol{u}_2^* &= [-2.805118,\ 3.131312]^\top, \\ \boldsymbol{u}_3^* &= [-3.779310,\ -3.283186]^\top, \\ \boldsymbol{u}_4^* &= [3.584428,\ -1.848126]^\top, \end{aligned}$$
each corresponding to the minimum value $J_H^* = 0$.
- **Beale's function:** The objective function $J_B(u_1, u_2)$, defined as
$$\begin{aligned} J_B(u_1, u_2) = J_{B,1}(u_1, u_2) + J_{B,2}(u_1, u_2) \\ + J_{B,3}(u_1, u_2), \end{aligned}$$
$$\begin{aligned} J_{B,1}(u_1, u_2) &= (1.5 - u_1 + u_1 u_2)^2, \\ J_{B,2}(u_1, u_2) &= (2.25 - u_1 + u_1 u_2^2)^2, \\ J_{B,3}(u_1, u_2) &= (2.625 - u_1 + u_1 u_2^3)^2, \end{aligned}$$
possesses a unique, well-defined global minimum surrounded by large flat regions, posing challenges for gradient-free methods that depend on local variation in function values for exploration. By analytical computation, the critical points of $J_B(u_1, u_2)$ are determined as follows:
$$\begin{aligned} &\boldsymbol{u}_1^* = [3,\ 0.5]^\top, \quad J_B(\boldsymbol{u}_1^*) = 0, \\ &\boldsymbol{u}_2^* \approx [0.1005, -2.6445]^\top, \quad J_B(\boldsymbol{u}_2^*) \approx 9.8645, \\ &\boldsymbol{u}_3^* = [0,\ 1]^\top, \quad J_B(\boldsymbol{u}_3^*) = 14.2031. \end{aligned}$$
The first critical point corresponds to the global minimum of the function, whereas the remaining two critical points are verified to be saddle points.
- **Six-Hump Camel Back function:**
$$\begin{aligned} J_S(u_1, u_2) = (4 - 2.1u_1^2 + u_1^{4/3})u_1^2 + u_1 u_2 \\ + (-4 + 4u_2^2)u_2^2 \end{aligned}$$
is a global optimization test function. Within the bounded region are six local minima, two of them are global minima:
$$\begin{aligned} \boldsymbol{u}_1^* &= [-0.0898,\ 0.7126]^\top, \\ \boldsymbol{u}_2^* &= [0.0898,\ -0.7126]^\top, \end{aligned}$$
and the minimum $J_S^* = -1.0316$.
- **Rosenbrock's function:**
$$J_R(u_1, u_2) = (1 - u_1)^2 + 100(u_2 - u_1^2)^2$$
(often referred to as the "banana function") features a narrow, curved valley leading to a global minimum. It is commonly used to evaluate convergence speed and stability in ill-conditioned optimization landscapes. By calculation, the critical points of $J_R(u_1, u_2)$ are
$$\begin{aligned} &\boldsymbol{u}_1^* = [1,\ 1]^\top, \quad J_R(\boldsymbol{u}_1^*) = 0, \\ &\boldsymbol{u}_2^* = [-1,\ 1]^\top, \quad J_R(\boldsymbol{u}_2^*) = 4. \end{aligned}$$
The first optimal solution is a global minimum, while the second optimal solution is a saddle point.

Collectively, these test functions encompass multi-modality, strong coupling, nonconvexity, and flatness — key challenges frequently encountered in practical optimization and control problems — thereby providing a comprehensive assessment of the proposed algorithm's performance.

The linear subsystem is similar to (32) with $a = -0.5$, $b = 1$, $c = 2$ and initial $x_0 = 0$. The observation noise is an ARMA process defined as (33).

For each test function, both the initial value points $\hat{\boldsymbol{u}}_0$ and the fixed points $\boldsymbol{u}^0$ are sampled within the following

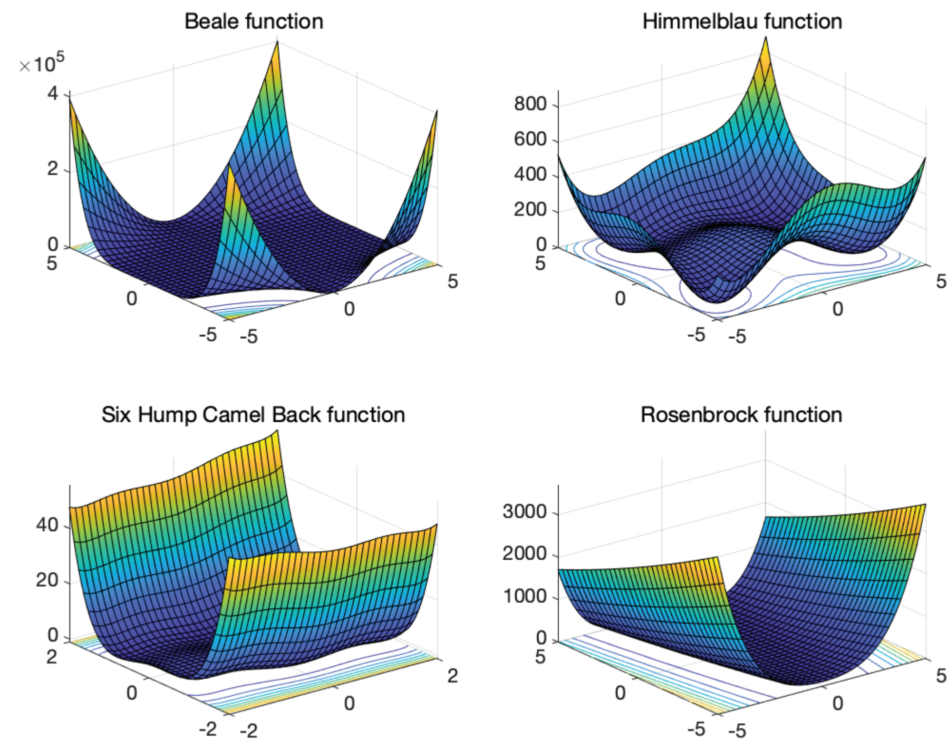

(a) The surface plots of the test functions.

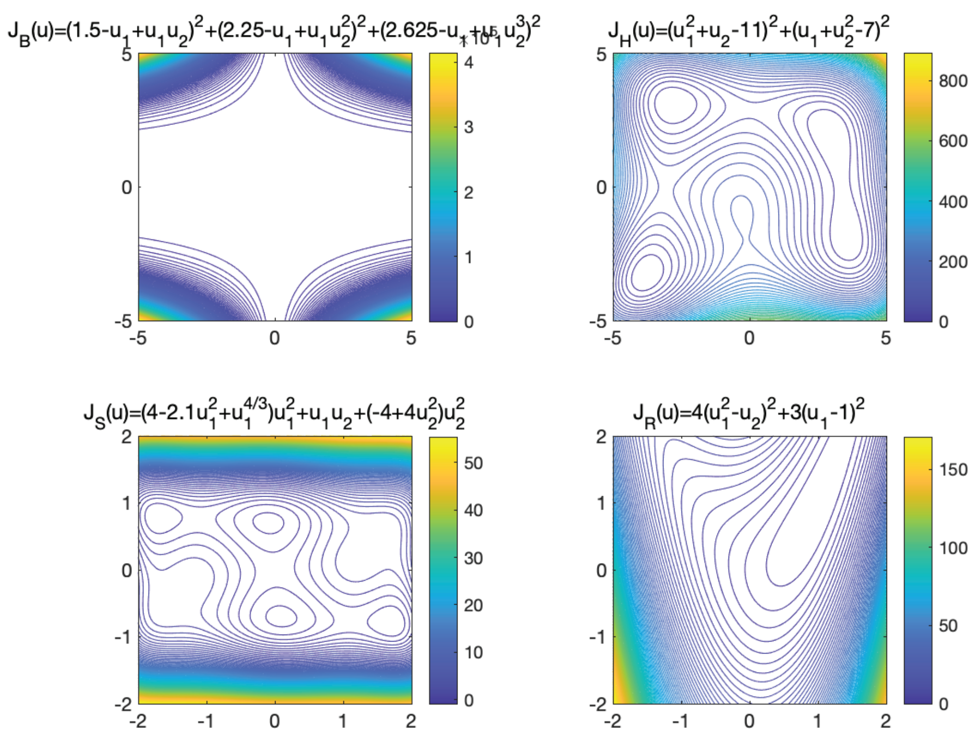

(b) The contour plots of the test functions.

Fig. 6. The test functions for ESC of the MISO Hammerstein system.

bounded rectangular domains:

- Himmelblau: $\hat{\boldsymbol{u}}_0 \sim \mathcal{U}(-5,5)$, $\boldsymbol{u}^0 \sim \mathcal{U}(-5,5)$;
- Beale: $\hat{\boldsymbol{u}}_0 \sim \mathcal{U}(-4,4)$, $\boldsymbol{u}^0 \sim \mathcal{U}(-4,4)$;
- Six-Hump Camel Back: $\hat{\boldsymbol{u}}_0 \sim \mathcal{U}(-2,2)$, $\boldsymbol{u}^0 \sim \mathcal{U}(-2,2)$;
- Rosenbrock: $\hat{\boldsymbol{u}}_0 \sim \mathcal{U}(-2,2)$, $\boldsymbol{u}^0 \sim \mathcal{U}(-2,2)$.

For each case, 10 independent groups of random points are generated to ensure statistical reliability.

The algorithm employs a step-size sequence $\gamma_k = 1/k$ and a smoothing parameter sequence $\alpha_k = \alpha_0/k^{\alpha}$, $k = 1, 2, \dots, K$, where the baseline smoothing parameter is set to $\alpha_0 = 1.5$ and the decay exponent to $\alpha = 0.3$. Two types of stochastic perturbations are applied, controlled by a binary flag $\in \{0, 1\}$ that takes values 0 and 1 with equal probability $1/2$:

- If flag $= 0$: uniformly distributed random perturbations are used, with

$$M_k = 1 + k^{1/3}.$$

- If flag $= 1$: normally distributed random perturbations are used, with

$$M_k = \ln(k+1).$$

All numerical simulations are executed for $K = 2000$ steps.

The trajectories of the estimates $\hat{\boldsymbol{u}}_k$ and the output z_k of the MISO Hammerstein system versus the iteration steps k for the four test functions under different scenarios are shown in Fig. 7.

From the simulations, we observe that by selecting the appropriate α_k, the algorithm can effectively explore the extremum of the mapping Q, even in nonconvex scenarios. The fixed point $\boldsymbol{u}^0$ can also be regarded as priori knowledge of the extreme point. By varying $\boldsymbol{u}^0$, distinct extrema can be explored.

Here the steady-state input–output mapping is $y = Q(\boldsymbol{u}) = \frac{4}{3}J(u_1, u_2)$, thus minimizing Q is equivalent to minimizing J. However, if $c = 2$ is set to -2 for example, the algorithm will seek the maximum of J.

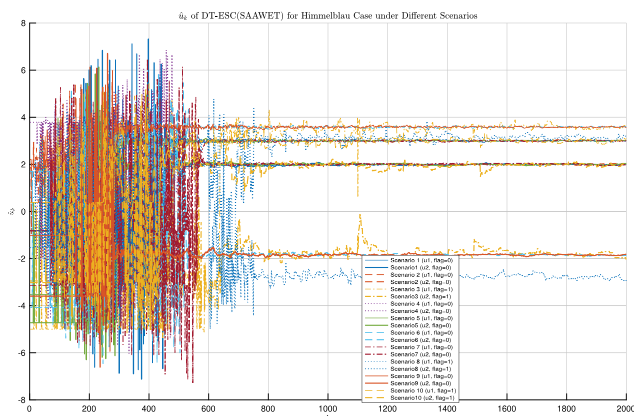

(a) Estimates $\hat{\boldsymbol{u}}_k$ for Himmelblau case

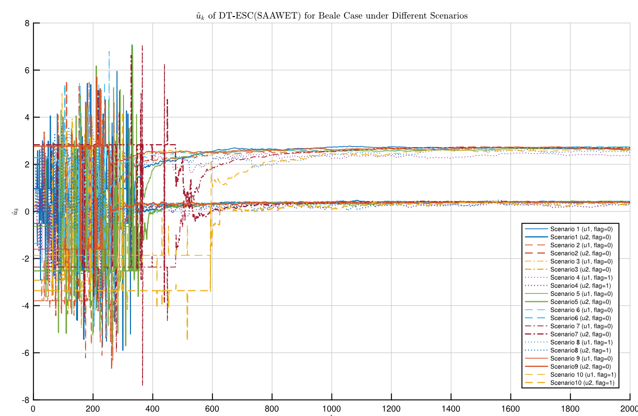

(b) Estimates $\hat{\boldsymbol{u}}_k$ for Beale case

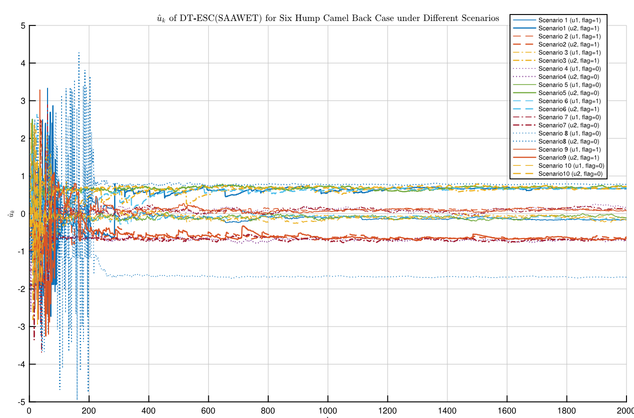

(c) Estimates $\hat{\boldsymbol{u}}_k$ for Six-Hump Camel Back case

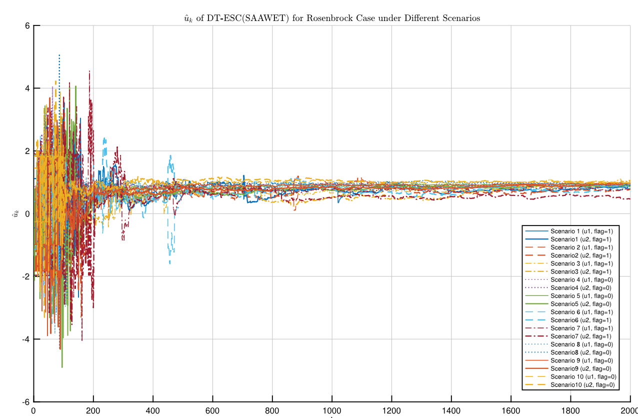

(d) Estimates $\hat{\boldsymbol{u}}_k$ for Rosenbrock case

Fig. 7. Estimates $\hat{\boldsymbol{u}}_k$ and output z_k of the SAAWET ESC for the test functions.

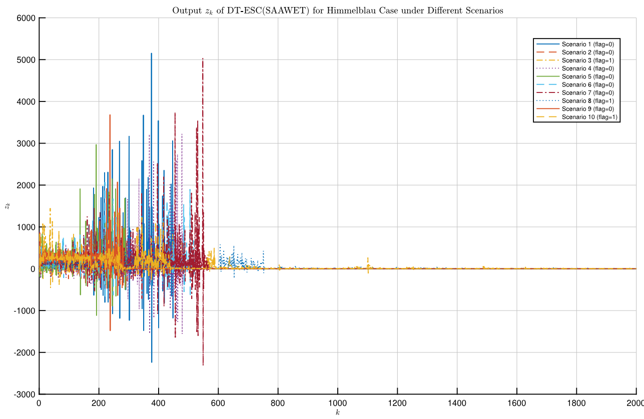

(e) Output z_k for Himmelblau case

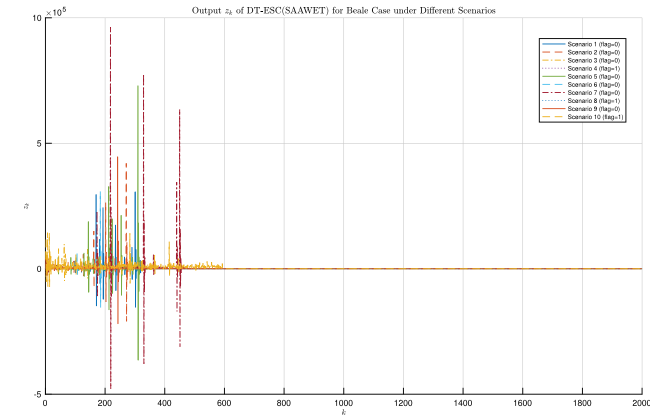

(f) Output z_k for Beale case

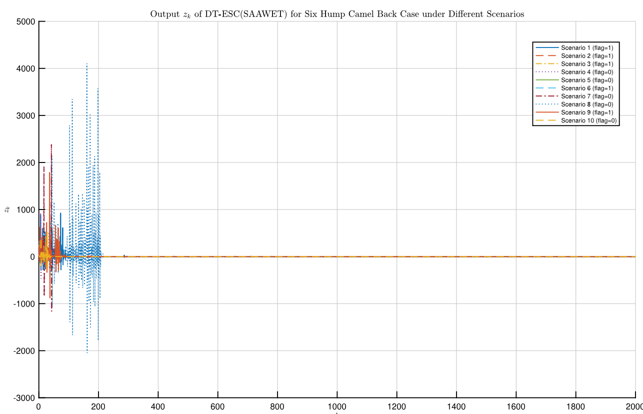

(g) Output z_k for Six-Hump Camel Back case

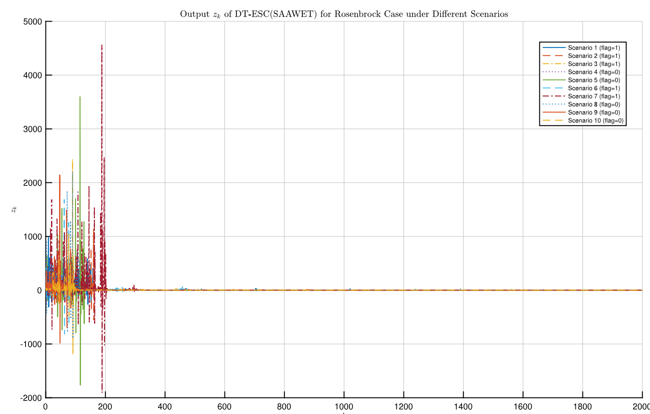

(h) Output z_k for Rosenbrock case

Fig. 7. (*Continued*)

Now, consider a two-input, two-state, one-output Hammerstein system with the following LTI subsystem:

$$\boldsymbol{x}_k = \begin{bmatrix} 0 & 1/2 \\ -1/2 & 0 \end{bmatrix} \boldsymbol{x}_{k-1} + \boldsymbol{v}_{k-1}, \quad y_k = [2,1]\boldsymbol{x}_k,$$

where $\boldsymbol{v}_k = [v_1(\boldsymbol{u}_k), v_2(\boldsymbol{u}_k)]^\top$ with $v_1(\boldsymbol{u}) = J_B(u_1,u_2)$ and $v_2(\boldsymbol{u}) = J_S(u_1,u_2)$. It is straightforward to verify that the matrix A is stable, and the system is both controllable and observable. The steady-state gain matrix of the LTI subsystem (from inputs to output) is given by

$$C(I-A)^{-1}B = [2,1]\begin{bmatrix} 0.8 & 0.4 \\ -0.4 & 0.8 \end{bmatrix}\begin{bmatrix} 1 & 0 \\ 0 & 1 \end{bmatrix} = [1.2, 1.6].$$

The scatter plot of the solution structure minimizing J_B or J_S, corresponding to the bi-objective optimization problem

$$\min_{u_1\in[-3,3],\, u_2\in[-2,2]} \{\boldsymbol{J}(\boldsymbol{u}) = [J_B(u_1,u_2), J_S(u_1,u_2)]^\top\}, \tag{34}$$

is shown in Fig. 8, where the optimal solution of the weighted minimization

$$\min_{u_1\in[-3,3],\, u_2\in[-2,2]} \{J_\lambda(\boldsymbol{u}) = 1.2\,J_B(\boldsymbol{u}) + 1.6 J_S(\boldsymbol{u})\} \tag{35}$$

is also plotted. The Pareto front of (34) is presented in Fig. 9.

The algorithm parameters are set as $\gamma_k = 1/k$ and $\alpha_k = 1.5/k^{0.3}$, $k = 1,2,\ldots,K$, with a uniformly distributed stochastic dither $M_k = 1 + k^{1/3}$. The observation noise is the same as in (33). The initial estimate is set to $\hat{\boldsymbol{u}}_0 = [-2,3]^\top$, the reset point is $\boldsymbol{u}^0 = [2,2]^\top$, and the initial state is fixed at $\boldsymbol{x}_0 = \boldsymbol{0}$. The total number of steps is $K = 2000$.

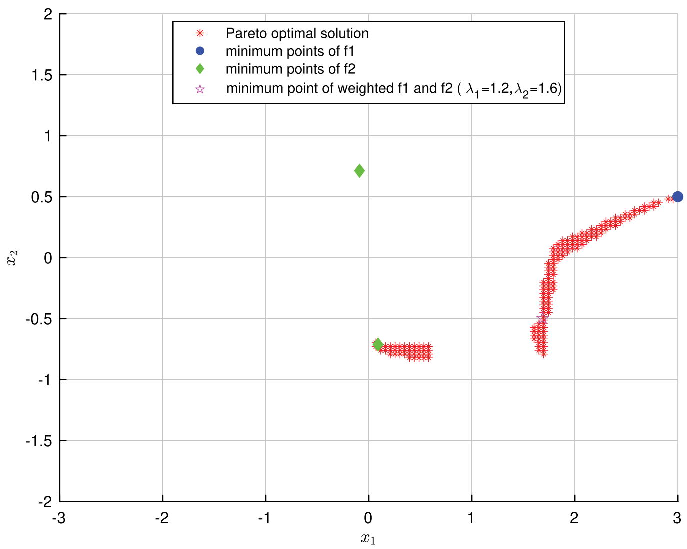

Fig. 8. The scatter plot of solution structure of J_B and J_S.

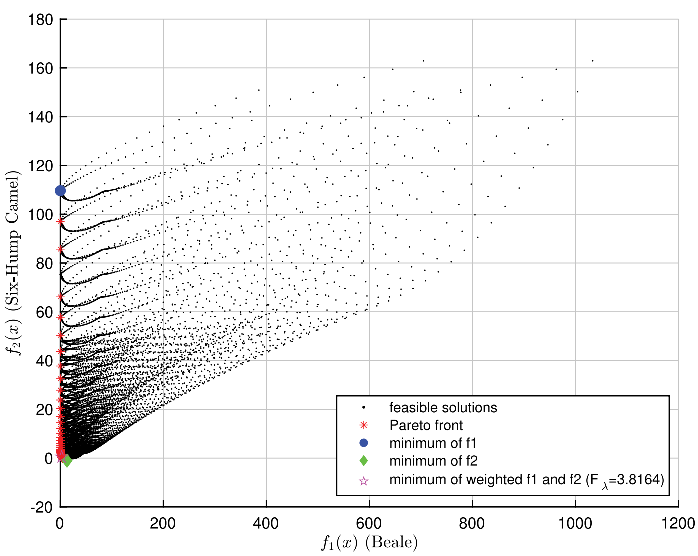

Fig. 9. The scatter plot of Pareto front of $[J_B, J_S]$.

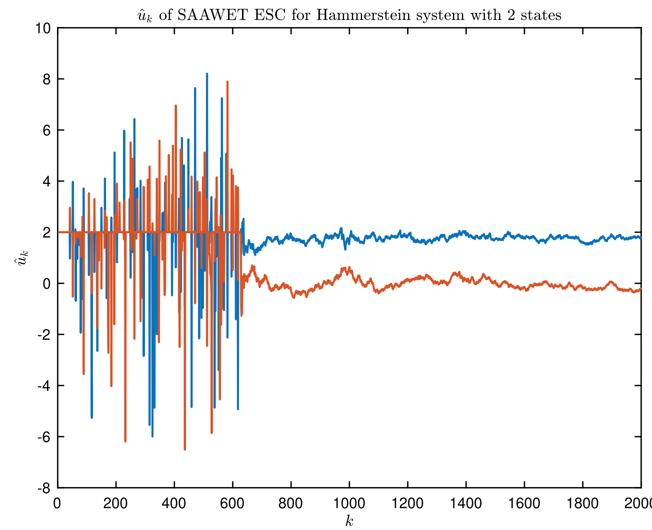

Fig. 10. Estimates $\hat{\boldsymbol{u}}_k$ of the SAAWET ESC for a MISO Hammerstein system with two states.

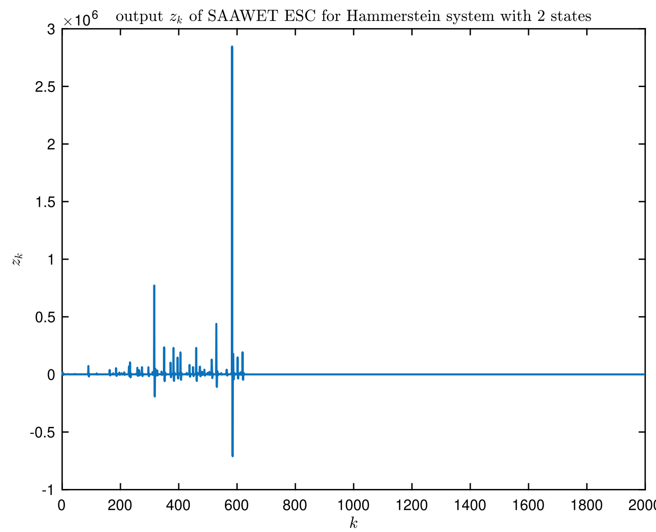

Fig. 11. Output z_k of the MISO Hammerstein system with two states.

The trajectories of the estimate $\hat{\boldsymbol{u}}_k$ and the output z_k of the two-state MISO Hammerstein system versus the iteration steps k are shown in Figs. 10 and 11, respectively. It is observed that the estimate $\hat{\boldsymbol{u}}_k$ converges asymptotically to the Pareto-optimal solution of (35).

5.3. *Application to material balance control of CSTR*

A CSTR is a well-mixed chemical reactor in which reactants are continuously fed while products are continuously removed, maintaining a constant reactor volume. Perfect mixing is assumed, so that temperature and species concentrations are uniform throughout the reactor and equal to those at the outlet. Due to its nonlinear dynamics — particularly for exothermic reactions with heat exchange — CSTRs are widely used as benchmark systems in nonlinear control and optimization studies.

A CSTR model is employed here to characterize a non-isothermal, irreversible first-order exothermic reaction A $\rightarrow$ B occurring within the reactor. Specifically, we consider the well-established CSTR model [18], which is governed by the following set of continuous-time nonlinear differential equations:

$$\frac{\mathrm{d}C_A}{\mathrm{d}t} = \frac{q}{V}(C_{A0} - C_A) - k_0 C_A \mathrm{e}^{-\frac{E}{RT}}, \tag{36}$$

$$\frac{\mathrm{d}T}{\mathrm{d}t} = \frac{q}{V}(T_0 - T) - \frac{\Delta H}{\rho C_p} k_0 C_A \mathrm{e}^{-\frac{E}{RT}} + \frac{\rho_c C_{pc}}{\rho C_p V} q_c \left(1 - \mathrm{e}^{-\frac{h_A}{\rho_c C_{pc} q_c}}\right)(T_{c0} - T), \tag{37}$$

where C_A (mol/L) denotes the outlet concentration of reactant A, T (K) is the reactor temperature, q_c (L/min) represents the coolant flow rate, and C_{A0} (mol/L) is the inlet feed concentration of A.

The control objective is to achieve precise material balance for species A by adjusting the coolant flow rate q_c and regulating the feed concentration C_{A0}. To quantify this objective, we minimize the absolute steady-state error of the material balance for A, defined as

$$J = \left| q(C_{A0,\mathrm{ss}} - C_{A,\mathrm{ss}}) - k_0 C_{A,\mathrm{ss}} \mathrm{e}^{-\frac{E}{RT_{\mathrm{ss}}}} V \right|, \tag{38}$$

the subscript ss on $C_{A0,\mathrm{ss}}$, $C_{A,\mathrm{ss}}$, and T_{ss} denotes their steady-state values under the stationary operating conditions of the stochastic process. In this cost function, the term $q(C_{A0,\mathrm{ss}} - C_{A,\mathrm{ss}})$ represents the molar flow rate of unreacted species A at the reactor outlet under steady state, while the term $k_0 C_{A,\mathrm{ss}} \mathrm{e}^{-\frac{E}{RT_{\mathrm{ss}}}} V$ describes the molar consumption rate of A resulting from the exothermic reaction.

The nominal model parameters are listed in Table 1. The sampling period is $T_s = 0.01$ min and the total simulation duration is 15 min. The initial values for (36) and (37) are $C_A(0)$ and $T(0) = 438.5$ K.

The above CSTR process has been widely modeled as a Hammerstein-type system, as discussed, for example, in [19]. After discretization, the process described by (36) and (37) can be accurately approximated by a two-input, three-output Hammerstein–Wiener model. In this formulation, the inputs are $\boldsymbol{u} = [q_c, C_{A0}]^\top$, the outputs are $\boldsymbol{y} = [C_{A0}, C_A, T]^\top$, and the nonlinear mapping $h(\cdot)$ is defined by the objective function in (38).

Table 1. CSTR model parameters.

Parameter	Value	Description
q	100 L/min	Feed flow rate
V	100 L	Reactor volume
k_0	$7.2 \times 10^{10}\,\mathrm{min}^{-1}$	Pre-exponential factor
E/R	1×10^4 K	Activation energy term
ΔH	-2×10^5 cal/mol	Heat of reaction
ρ	1×10^3 g/L	Reaction fluid density
C_p	1 cal/(gK)	Heat capacity of fluid
ρ_c	1×10^3 g/L	Coolant density
C_{pc}	1 cal/(gK)	Heat capacity of coolant
h_A	7×10^5 cal/(min K)	Heat transfer term
T_0	350 K	Feed temperature
T_{c0}	350 K	Coolant inlet temperature
q_c	$[50, 150]$ L/min	Coolant flow rate
C_{A0}	$[0.5, 1.5]$ mol/L	Feed concentration

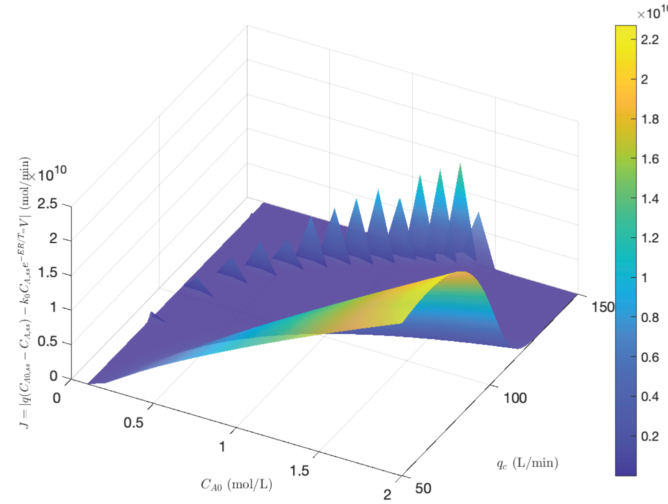

Fig. 12. The surface graph of J with respective to q_c and C_{A0}.

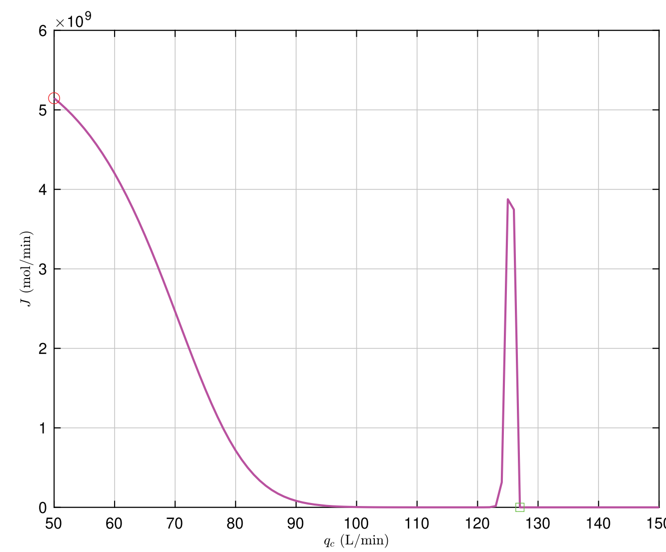

Fig. 13. A slice plot of J at $C_{A0} = 0.5$.

To visualize the steady-state behavior, we plotted the surface of the objective function J with respect to q_c and C_{A0} using the parameters in Table 1, as shown in Fig. 12. Additionally, a slice plot at $C_{A0} = 0.5$ is provided in Fig. 13. These figures clearly illustrate that the optimization problem is nonconvex and nonsmooth, which highlights the challenges for ESC.

Assuming the inputs are constrained as $q_c \in [50, 150]$ L/min and $C_{A0} \in [0.5, 1.5]$ mol/L, we apply Algorithms (20), (13), and (19) to investigate the ESC problem for the CSTR model. The step-size sequence is chosen as $\gamma_k = 0.01/k$, and the smoothing parameter sequence is configured as $\alpha_k = \alpha_0/k^\alpha$, with $\alpha = 0.3$ and $\alpha_0 = 0.1$ for the estimate $\hat{q}_{c,k}$, and

$\alpha_0 = 0.3$ for the estimate $\hat{C}_{A0,k}$. A uniformly distributed random perturbation is employed to explore the input space.

For comparison, the classical ESC algorithm using deterministic sinusoidal perturbation and synchronous demodulation for gradient estimation is also implemented [11].

$$q^{\text{esc}}_{c,k-1} = \hat{q}^{\text{esc}}_{c,k-1} + a_{qc}\sin(\omega t_k),$$

$$C^{\text{esc}}_{A0,k-1} = \hat{C}^{\text{esc}}_{A0,k-1} + a_{CA0}\sin(\omega t_k + \pi/2),$$

$$\hat{q}^{\text{esc}}_{c,k} = \hat{q}^{\text{esc}}_{c,k-1} - T_s\gamma_{qc}\frac{2}{\pi}\frac{J_k\sin(\omega t_k)}{a_{qc}},$$

$$\hat{C}^{\text{esc}}_{A0,k} = \hat{C}^{\text{esc}}_{A0,k-1} - T_s\gamma_{CA0}\frac{2}{\pi}\frac{J_k\sin(\omega t_k + \pi/2)}{a_{CA0}}.$$

where t_k is the sampling time, and J_k is the transient value of the objective function (38) obtained by replacing the steady-state variables with the current variable estimates. The algorithm parameters are set as follows:

$$\omega = 10; \quad a_{qc} = 0.5, \quad a_{CA0} = 0.1;$$

$$\gamma_{qc} = 0.5, \quad \gamma_{CA0} = 0.01.$$

The trajectories of the control variables $\hat{q}_{c,k}$ and $\hat{C}_{A0,k}$, together with the transient objective function values J_k versus the iteration steps k for both algorithms, are shown in Fig. 14, while the corresponding system outputs are illustrated in Fig. 15.

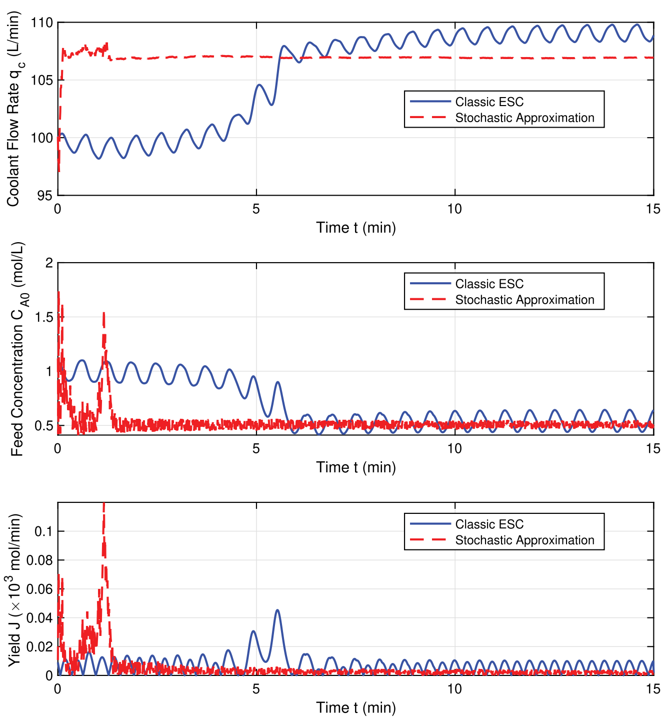

Fig. 14. Estimates $\hat{\boldsymbol{u}}_k$ of the SAAWET ESC.

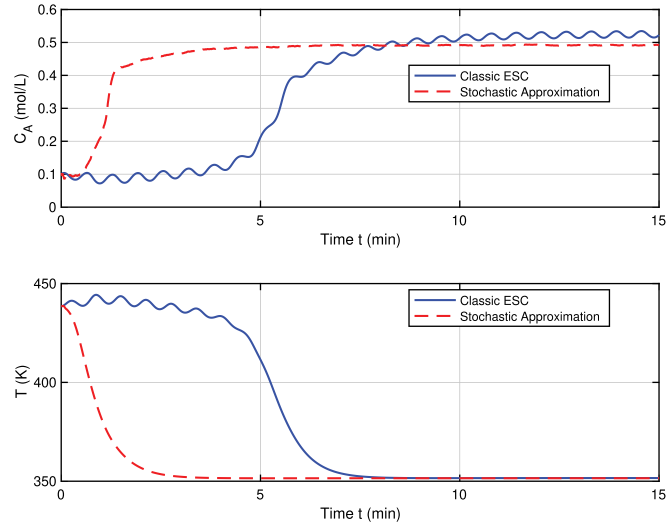

Fig. 15. Output z_k of the MISO Hammerstein system.

It was observed that both algorithms converge to near-nominal optimal inputs; however, the proposed algorithm converges directly to the optimal values, whereas the perturbation-based ESC using deterministic dithers reaches only a small neighborhood around the optimum due to the presence of the deterministic perturbations, clearly illustrating the difference between the two techniques.

6. Concluding Remarks

This paper presented a discrete-time ESC framework for MISO Hammerstein systems with unknown linear dynamics and nonconvex, high-dimensional cost functions. By combining stochastic approximation algorithm with expanding truncations, the method guarantees bounded iterates and closed-loop stability under noisy, dynamically filtered measurements. Convergence to the set of stationary points from arbitrary initial conditions is established, demonstrating robust performance in complex optimization landscapes with multiple extrema. Simulation studies confirm the algorithm's effectiveness in navigating high-dimensional inputs while maintaining stable behavior. These results provide a rigorous and practical foundation for real-time optimization of MISO systems, with potential extensions toward directed convergence to local minima and distributed multi-agent implementations.

Acknowledgments

The first author was supported by the China Scholarship Council (No. 202306060084) and the Fundamental Research Funds for the Central Universities (No. DUT25Z2703); and the second author was supported by the China Scholarship Council (No. 202308210291). The work of the first two

authors was completed during their visit to the University of Melbourne.

Appendix A. Noise Analysis of the SAAWET ESC Algorithm

In this appendix, we present the noise analysis of the SAAWET ESC algorithm (21) and (23), that is, we prove that (31) holds. We primarily provide the proof for the case of uniformly distributed perturbations; the proof for the normally distributed case follows by a similar method.

Lemma A.1. *Assume that Assumptions* 1–3 *and Conditions* 1, 2, *and* 4 *hold. Let* $\boldsymbol{w}_k \sim \mathcal{U}(\partial\mathcal{B})$ *be i.i.d. Then almost surely*

$$\lim_{k\to\infty} \boldsymbol{\xi}_k^{(1)} = 0. \tag{A.1}$$

Proof. Note that $\boldsymbol{w}_k = [w_k^1, \dots, w_k^m]^\top \sim \mathcal{U}(\partial\mathcal{B})$ is a sequence of i.i.d. uniformly distributed random vectors with zero mean. By using the Taylor series expansion, we have

$$\begin{aligned} &Q(\hat{\boldsymbol{u}}_{k-1} + \alpha_k \boldsymbol{w}_k) - Q(\hat{\boldsymbol{u}}_{k-1}) \\ &\quad = \alpha_k \boldsymbol{w}_k^\top \nabla Q(\hat{\boldsymbol{u}}_{k-1}) + o(\alpha_k), \end{aligned}$$

Thus,

$$\begin{aligned} &\mathrm{E}\left[\frac{Q(\hat{\boldsymbol{u}}_{k-1} + \alpha_k \boldsymbol{w}_k)}{\alpha_k} \boldsymbol{w}_k \middle| \mathscr{F}_{k-1} \right] \\ &\quad = \mathrm{E}\left[\frac{Q(\hat{\boldsymbol{u}}_{k-1} + \alpha_k \boldsymbol{w}_k) - Q(\hat{\boldsymbol{u}}_{k-1})}{\alpha_k} \boldsymbol{w}_k \middle| \mathscr{F}_{k-1} \right] \\ &\quad = \mathrm{E}\left[\boldsymbol{w}_k \boldsymbol{w}_k^\top \nabla Q(\hat{\boldsymbol{u}}_{k-1}) \middle| \mathscr{F}_{k-1} \right] + o(1). \end{aligned}$$

The result follows by noticing that $\hat{\boldsymbol{u}}_{k-1}$ is $\mathscr{F}_{k-1}$-measurable, w_k is independent of $\mathscr{F}_{k-1}$, and $\mathrm{E}[\boldsymbol{w}_k \boldsymbol{w}_k^\top] = I$. □

Lemma A.2. *Assume that Assumptions* 1–3 *and Conditions* 1, 2, *and* 4 *hold. There is* Ω *with* $\mathrm{P}\{\Omega\} = 1$, *such that if* $\omega \in \Omega$ *and if* $\{\hat{\boldsymbol{u}}_{n_k-1}\}$ *is a bounded subsequence of* $\{\hat{u}_k\}$, *then*

$$\lim_{T\to 0} \limsup_{k\to\infty} \frac{1}{T} \left\| \sum_{i=n_k}^{m(n_k,T)} \gamma_i \boldsymbol{\xi}_i^{(2)} \right\| = 0. \tag{A.2}$$

Lemma A.3. *Assume that Assumptions* 1–3 *and Conditions* 1, 2, *and* 4 *hold. Let* $\boldsymbol{w}_k \sim \mathcal{U}(\partial\mathcal{B})$ *be i.i.d., and set* $M_k = k^{1/(1+\mu)}$. *Let* $\lambda \in (0,1)$. *Then, for any* $j = 0, 1, \dots, [k^{\lambda/(1+\mu)}]$, $\sum_{i=k}^{k+j} \gamma_i \xrightarrow[k\to\infty]{} 0$, *and*

$$\begin{aligned} &\sum_{i=k}^{k+j} \frac{\gamma_i \|\boldsymbol{x}_{i-\ell}\| \boldsymbol{w}_i}{\alpha_i} \xrightarrow[k\to\infty]{} 0, \quad \ell = 0, 1, \\ &\sum_{i=k}^{k+j} \frac{\gamma_i e_i \boldsymbol{w}_i}{\alpha_i} \xrightarrow[k\to\infty]{} 0. \end{aligned} \tag{A.3}$$

where $[a]$ *denotes the integer part of the real number* a, *and* μ *is given in Assumption* 1.

Proof. The result $\sum_{i=k}^{k+j} \gamma_i \xrightarrow[k\to\infty]{} 0$ is straightforward to verify, see [20, Lemma 2].

It follows from (21)–(23) and Condition 2 that

$$\begin{aligned} &\sigma_k \le k \quad \text{and} \\ &\|\hat{\boldsymbol{u}}_k\| \le M_{\sigma_{k-1}} \le M_{k-1} = (k-1)^{1/(1+\mu)}. \end{aligned} \tag{A.4}$$

By Condition 2 and Assumption 1, it follows that there is $c_1 > 0$ such that

$$\|\boldsymbol{J}(\hat{\boldsymbol{u}}_{k-1} + \alpha_k \boldsymbol{w}_k)\| \le c_1 k^{\mu/(1+\mu)}, \quad \forall\, k \ge 1. \tag{A.5}$$

By stability of matrix A, there is a constant $c_2 > 0$ such that

$$\|\boldsymbol{x}_k\| \le c_2 k^{\mu/(1+\mu)}, \quad \forall\, k \ge 1. \tag{A.6}$$

Therefore,

$$\begin{aligned} &\sum_{i=k}^{k+j} \gamma_i \|\boldsymbol{x}_{i-\ell}\| / \alpha_i \\ &\quad \le c_2 \sum_{i=k}^{k+[k^{\lambda/(1+\mu)}]} i^{-1+\mu/(1+\mu)+\alpha} \\ &\quad \le c_2 \sum_{i=k}^{k+[k^{\lambda/(1+\mu)}]} \int_{i-1}^{i} \frac{\mathrm{d}x}{x^{1/(1+\mu)-\alpha}} \\ &\quad = c_2 \frac{1}{\mu/(1+\mu)+\alpha} (k-1)^{\mu/(1+\mu)+\alpha} \\ &\qquad \cdot \left[\left(1 + \frac{[k^{\lambda/(1+\mu)}]+1}{k-1} \right)^{\mu/(1+\mu)+\alpha} - 1 \right] \\ &\quad \xrightarrow[k\to\infty]{} 0 \end{aligned}$$

since $\lambda \in (0,1)$ and $\alpha < \frac{1}{1+\mu}$.

Finally, the second limit in (A.3) follows from Condition 4. □

Lemma A.4 (Analysis of noise $\boldsymbol{\xi}_k^{(3)}$). *Assume that Assumptions* 1–3 *and Conditions* 1, 2, *and* 4 *hold. Let* $\boldsymbol{w}_k \sim \mathcal{U}(\partial\mathcal{B})$ *be i.i.d., and set* $M_k = k^{1/(1+\mu)}$. *Then* (31) *holds for* $\ell = 3$ *and any* $\{n_k\}$ *such that* $\hat{\boldsymbol{u}}_{n_k-1}$ *converges.*

Proof. By substituting the linear subsystem Eqs. (4) into (30), we find that

$$\boldsymbol{\xi}_k^{(3)} = C(I-A)^{-1} A(\boldsymbol{x}_{k-1} - \boldsymbol{x}_k) \boldsymbol{w}_k / \alpha_k, \tag{A.7}$$

the noise is related to the state x_k, it suffices to show

$$\lim_{T\to 0} \limsup_{k\to\infty} \frac{1}{T} \left\| \sum_{i=n_k}^{m(n_k,T)} \frac{\gamma_i (\|\boldsymbol{x}_{i-1} - \boldsymbol{x}_i\|) \boldsymbol{w}_i}{\alpha_i} \right\| = 0.$$

By decomposing $\sum_{i=n_k}^{m(n_k,T)} \frac{\gamma_i(\|\boldsymbol{x}_{i-1}-\boldsymbol{x}_i\|)\boldsymbol{w}_i}{\alpha_i}$ as

$$\sum_{i=n_k}^{n_k+[n_k^{\lambda/(1+\mu)}]} \frac{\gamma_i(\|\boldsymbol{x}_{i-1}-\boldsymbol{x}_i\|)w_i}{\alpha_i} + \sum_{i=n_k+[n_k^{\lambda/(1+\mu)}]+1}^{m(n_k,T)} \frac{\gamma_i(\|\boldsymbol{x}_{i-1}-\boldsymbol{x}_i\|)\boldsymbol{w}_i}{\alpha_i}$$

we can derive from Lemma A.3 that its first term tends to zero as $k \to \infty$.

Consequently, for proving the lemma, we only need to verify that

$$\frac{\|\boldsymbol{x}_{n_k+[n_k^{\lambda/(1+\mu)}]+j+1} - \boldsymbol{x}_{n_k+[n_k^{\lambda/(1+\mu)}]+j}\|}{\alpha_{n_k+[n_k^{\lambda/(1+\mu)}]+j+1}} \xrightarrow[k\to\infty]{} 0 \tag{A.8}$$

for $j = 0, 1, \dots, m(n_k, T) - n_k - [n_k^{\lambda/(1+\mu)}] - 1$.

Note that under Assumption 2: A is a stable matrix, there exist constants $c_0 > 0$ and $\delta > 0$ such that

$$\|A^k\| \leq c_0 \mathrm{e}^{-\delta k}, \quad \forall\, k \geq 0. \tag{A.9}$$

By performing recursions on the first equation of (4), we obtain

$$\begin{aligned}\boldsymbol{x}&_{n_k+[n_k^{\lambda/(1+\mu)}]+j+1} \\ &= A^{[n_k^{\lambda/(1+\mu)}]+j+1}\boldsymbol{x}_{n_k-1} \\ &\quad + \sum_{i=n_k-1}^{n_k+[n_k^{\lambda/(1+\mu)}]+j-1} A^{n_k+[n_k^{\lambda/(1+\mu)}]+j-i-1} \\ &\quad \times B\boldsymbol{J}(\boldsymbol{u}_i).\end{aligned}$$

Then, using the triangle inequality, we derive the following estimate

$$\begin{aligned}\|\boldsymbol{x}&_{n_k+[n_k^{\lambda/(1+\mu)}]+j+1} - \boldsymbol{x}_{n_k+[n_k^{\lambda/(1+\mu)}]+j}\| \\ &\leq \|A^{[n_k^{\lambda/(1+\mu)}]+j+1}(A-I)\boldsymbol{x}_{n_k-1}\| \\ &\quad + \|A^{[n_k^{\lambda/(1+\mu)}]+j+1}B\boldsymbol{J}(\boldsymbol{u}_{n_k})\| \\ &\quad + \Bigg\|\sum_{i=n_k-1}^{n_k+[n_k^{\lambda/(1+\mu)}]+j+1} A^{n_k+[n_k^{\lambda/(1+\mu)}]+j-i+1} \\ &\quad \times B[\boldsymbol{J}(\boldsymbol{u}_{i+1}) - \boldsymbol{J}(\boldsymbol{u}_i)]\Bigg\|.\end{aligned} \tag{A.10}$$

The first term on the right-hand side (RHS) of (A.10) is bounded by

$$c_0 \mathrm{e}^{-\delta n_k + [n_k^{\lambda/(1+\mu)}]+j+1} |c_0 \mathrm{e}^{-\delta} - 1| c_2 n_{k-1}^{\mu/(1+\mu)},$$

which tends to zero as $k \to \infty$. The second term on the RHS of (A.10) also approaches zero by (A.9), (3) and the boundedness of $\boldsymbol{u}_{n_k-1}$. Finally, the last term on the RHS of (A.10) is bounded by

$$\frac{c_0\|B\|}{1-\mathrm{e}^{-\delta}} \max_{n_k-1 \leq i \leq m(n_k,T)} \|\boldsymbol{J}(\boldsymbol{u}_{i+1}) - \boldsymbol{J}(\boldsymbol{u}_i)\|.$$

A standard analysis of the SAAWET algorithm [16, Step 2 on the proof of Theorem 2.2.1] can prove that

$$\lim_{k\to\infty} \max_{n_k-1 \leq i \leq m(n_k,T)} \|\hat{\boldsymbol{u}}_{i+1} - \hat{\boldsymbol{u}}_i\| = 0,$$

From Assumption 1, $\boldsymbol{J}(\cdot)$ is continuous, and from Conditions 1 and 2, it follows that the last term on the RHS of (A.10) converges to zero as $k \to \infty$, hence the lemma is established. □

ORCID

Xing-Min Chen
https://orcid.org/0000-0001-8630-2883
Chao Gao
https://orcid.org/0000-0002-6187-3281
Ying Tan
https://orcid.org/0000-0001-8495-0246

References

[1] I. I. Ostrovskii, Extremum regulation, *Autom. Remote Control* **18** (1957) 900–907.
[2] M. Krstić and H.-H. Wang, Stability of extremum seeking feedback for general nonlinear dynamic systems, *Automatica* **36**(4) (2000) 595–601.
[3] Y. Tan, W. Moase, C. Manzie, D. Nešić and I. Mareels, Extremum seeking from 1922 to 2010, in *Proc. 29th Chinese Control Conf.* (IEEE, 2010), pp. 14–26.
[4] A. Scheinker, 100 years of extremum seeking: A survey, *Automatica* **161** (2024) 111481.
[5] Y. Tan, D. Nešić and I. Mareels, On non-local stability properties of extremum seeking control, *Automatica* **42**(6) (2006) 889–903.
[6] N. Mimmo, L. Marconi and G. Notarstefano, Uniform nonconvex optimization via extremum seeking, *IEEE Trans. Autom. Control* **69**(12) (2024) 8263–8276.
[7] A. Williams, M. Krstic and A. Scheinker, Semiglobal safety-filtered extremum seeking with unknown CBFs, *IEEE Trans. Autom. Control* **70**(3) (2025) 1698–1713.
[8] Y. Tan, D. Nešić, I. M. Mareels and A. Astolfi, On global extremum seeking in the presence of local extrema, *Automatica* **45**(1) (2009) 245–251.
[9] C. Manzie and M. Krstic, Extremum seeking with stochastic perturbations, *IEEE Trans. Autom. Control* **54**(3) (2009) 580–585.
[10] W. H. Moase and C. Manzie, Semi-global stability analysis of observer-based extremum-seeking for Hammerstein plants, *IEEE Trans. Autom. Control* **57**(7) (2012) 1685–1695.
[11] R. C. Shekhar, W. H. Moase and C. Manzie, Discrete-time extremum-seeking for Wiener–Hammerstein plants, *Automatica* **50**(12) (2014) 2998–3008.
[12] M. S. Radenkovic and J.-D. Park, Almost sure convergence of extremum seeking algorithm using stochastic perturbation, *Syst. Control Lett.* **94** (2016) 133–141.

[13] H. K. Khalil, *Nonlinear Systems*, 3rd edn. (Prentice Hall, 2002).

[14] J. C. Duchi, P. L. Bartlett and M. J. Wainwright, Randomized smoothing for stochastic optimization, *SIAM J. Optim.* **22**(2) (2012) 674–701.

[15] Y. Nesterov and V. Spokoiny, Random gradient-free minimization of convex functions, *Found. Comput. Math.* **17**(2) (2017) 527–566.

[16] H.-F. Chen, *Stochastic Approximation and Its Applications* (Kluwer Academic Publishers, Dordrecht, The Netherlands, 2002).

[17] X.-M. Chen and C. Gao, On the convergence of smoothed functional stochastic optimization algorithms, *IFAC-PapersOnLine*, **48**(28) (2015) 229–233.

[18] J. Du, C. Song and P. Li, Multilinear model control of Hammerstein-like systems based on an included angle dividing method and the MLD-MPC strategy, *Ind. Eng. Chem. Res.* **48**(8) (2009) 3934–3943.

[19] P. Menold, F. Allgöwer and R. Pearson, Nonlinear structure identification of chemical processes, *Comput. Chem. Eng.* **21** (1997) S137–S142.

[20] H.-F. Chen, Adaptive regulator for Hammerstein and Wiener systems with noisy observations, *IEEE Trans. Autom. Control* **52**(4) (2007) 703–709.